


## Research Article

# Nrf1 Is Endowed with a Dominant Tumor-Repressing Effect onto the Wnt/ $\beta$ -Catenin-Dependent and Wnt/ $\beta$ -Catenin-Independent Signaling Networks in the Human Liver Cancer

Jiayu Chen,<sup>1,2</sup> Meng Wang,<sup>1</sup> Yuancai Xiang,<sup>1,3</sup> Xufang Ru,<sup>1,4</sup> Yonggang Ren,<sup>1,5</sup> Xiping Liu,<sup>2</sup> Lu Qiu,<sup>1,6</sup> and Yiguo Zhang<sup>1</sup> 

<sup>1</sup>The Laboratory of Cell Biochemistry and Topogenetic Regulation, College of Bioengineering and Faculty of Sciences, Chongqing University, No. 174 Shazheng Street, Shapingba District, Chongqing 400044, China

<sup>2</sup>Department of Biochemistry and Molecular Biology, Zunyi Medical University, No. 6 Xuefu-Xi Road, Xinpu New District, Zunyi, 563000 Guizhou, China

<sup>3</sup>Department of Biochemistry and Molecular Biology, School of Basic Medical Sciences, Southwest Medical University, No. 1 at the First Section of Xianglin Road, Longmatan District, Luzhou, 646000 Sichuan, China

<sup>4</sup>Department of Neurosurgery, Southwest Hospital, Army (Third Military) Medical University, No. 29 Gaotanyan Street, Shapingba District, Chongqing 400038, China

<sup>5</sup>Department of Biochemistry, North Sichuan Medical College, No. 55 Dongshun Road, Gaoping District, Nanchong, 637000 Sichuan, China

<sup>6</sup>School of Life Sciences, Zhengzhou University, No. 100 Kexue Avenue, Zhengzhou, 450001 Henan, China

Correspondence should be addressed to Yiguo Zhang; [yiguozhang@cqu.edu.cn](mailto:yiguozhang@cqu.edu.cn)

Received 7 January 2020; Accepted 20 February 2020; Published 23 March 2020

Academic Editor: Manuela Curcio

Copyright © 2020 Jiayu Chen et al. This is an open access article distributed under the Creative Commons Attribution License, which permits unrestricted use, distribution, and reproduction in any medium, provided the original work is properly cited.

Our previous work revealed that Nrf1 $\alpha$  exerts a tumor-repressing effect because its genomic loss (to yield Nrf1 $\alpha$ <sup>-/-</sup>) results in oncogenic activation of Nrf2 and target genes. Interestingly,  $\beta$ -catenin is concurrently activated by loss of Nrf1 $\alpha$  in a way similar to  $\beta$ -catenin-driven liver tumor. However, a presumable relationship between Nrf1 and  $\beta$ -catenin is not yet established. Here, we demonstrate that Nrf1 enhanced ubiquitination of  $\beta$ -catenin for targeting proteasomal degradation. Conversely, knockdown of Nrf1 by its short hairpin RNA (shNrf1) caused accumulation of  $\beta$ -catenin so as to translocate the nucleus, allowing activation of a subset of Wnt/ $\beta$ -catenin signaling responsive genes, which leads to the epithelial-mesenchymal transition (EMT) and related cellular processes. Such silencing of Nrf1 resulted in malgrowth of human hepatocellular carcinoma, along with malignant invasion and metastasis to the lung and liver in xenograft model mice. Further transcriptomic sequencing unraveled significant differences in the expression of both Wnt/ $\beta$ -catenin-dependent and Wnt/ $\beta$ -catenin-independent responsive genes implicated in the cell process, shape, and behavior of the shNrf1-expressing tumor. Notably, we identified that  $\beta$ -catenin is not a target gene of Nrf1, but this CNC-bZIP factor contributes to differential or opposing expression of other critical genes, such as CDH1, Wnt5A, Wnt11A, FZD10, LEF1, TCF4, SMAD4, MMP9, PTEN, PI3K, JUN, and p53, each of which depends on the positioning of distinct cis-regulatory sequences (e.g., ARE and/or AP-1 binding sites) in the gene promoter contexts. In addition, altered expression profiles of some Wnt/ $\beta$ -catenin signaling proteins were context dependent, as accompanied by decreased abundances of Nrf1 in the clinic human hepatomas with distinct differentiation. Together, these results corroborate the rationale that Nrf1 acts as a *bona fide* dominant tumor repressor, by its intrinsic inhibition of Wnt/ $\beta$ -catenin signaling and relevant independent networks in cancer development and malignant progression.

## 1. Introduction

On the oxygenated earth, all of the cellular life forms have evolutionarily established a series of integral cytoprotective systems against various stresses, such that these living organisms are allowed for ecological adaptation to the changing environments during development, growth, and other life processes [1]. Hence, it is plausible that there exists at least a set of versatile defense mechanisms (e.g., redox signaling to antioxidant gene regulatory networks) against oxidative stress [1–3], which have been brilliantly orchestrated in the prokaryotic to eukaryotic organisms, in order to maintain cell homeostasis and organ integrity under normal physiological and pathophysiological conditions. Amongst them, an evolutionarily conserved family of the cap'n'collar (CNC) basic-region leucine zipper (bZIP) transcription factors is presented across distinct species from marine bacteria to humans [3–5]. The CNC-bZIP family comprises its founding member *Drosophila* Cnc protein, the *Caenorhabditis elegans* Skn-1, the vertebrate activator nuclear factor-erythroid 2 (NF-E2) p45, NF-E2-related factor 1 (Nrf1, including its long TCF11 and short Nrf1 $\beta$ /LCR-F1), Nrf2, and Nrf3, as well as the repressors Bach1 (BTB and CNC homology 1) and Bach2 [6, 7], together with the recently identified Nach (Nrf and CNC homology) proteins existing in marine bacteria to early-diverging metazoans [3, 4]. These CNC/Nach-bZIP family members share a common evolutionary ancestor with the Maf (musculoaponeurotic fibrosarcoma oncogene) family, including sMaf (small Maf) proteins [4]. They play a host of vital, and even indispensable, roles in regulating distinct subsets of target genes involved in antioxidant, detoxification, redox metabolism, proteasomal degradation, adaptive cytoprotection, and other physiopathological responses to diverse cellular stresses [6–8]. Such genes are regulated transcriptionally by a functional heterodimer of each CNC-bZIP factor (except Skn-1) with a cognate partner sMaf or another bZIP protein, which directly binds the antioxidant and electrophile response elements (AREs/EpREs) and/or other *cis*-regulatory homologues (e.g., AP-1 binding site) within the gene promoter regions [6, 7].

In mammals, Nrf1 and Nrf2 are two principal CNC-bZIP proteins with similar, but different, structural domains [6, 9]. By the neighbor-joining phylogenetic analysis, Nrf1 is unveiled to serve as a living fossil to be reminiscent of the early ancestral evolutionary stages of the CNC/Nach-bZIP family members [4]. This is due to the fact that Nrf1, rather than Nrf2, has a unique additive N-terminal domain (NTD) that enables the former CNC-bZIP protein to be anchored within the endoplasmic reticulum (ER) membranes [9, 10]. Once the portion of Nrf1 is topologically partitioned into the ER lumen, it is N-glycosylated to yield an inactive glycoprotein [10–12]. Subsequently, the lumenally glycosylated domain of Nrf1 is dynamically repositioned through p97-driven *retrotranslocation* machinery into the cytoplasmic side. Therein, Nrf1 is deglycosylated to generate a transient deglycoprotein, which is further proteolytically processed by cytosolic proteasomes and/or DDI-1/2 proteases to give rise to a mature N-terminally-truncated CNC-bZIP factor, before being unleashed from ER membranes to

translocate the nucleus and mediate transcriptional expression of ARE-driven genes (e.g., those encoding proteasomal subunits) [13–15]. By contrast with the membrane-bound Nrf1, the water-soluble Nrf2 is neither localized in the ER lumen nor N-glycosylated in this subcellular compartment [10]. Such distinctions between Nrf1 and Nrf2 dictate the discrepant capacity of both CNC-bZIP factors, in order to exert combinational, different, or even opposing functions in maintaining normal development and growth under robust homeostatic conditions.

However, Nrf2 has been generally accepted as a master regulator of ARE battery gene expression [8, 16], though it is, in fact, not absolutely necessary for normal development and healthy growth [17]. This is corroborated by the fact that global *Nrf2*<sup>-/-</sup> knockout mice are viable and fertile, without any obvious defects and pathological phenotypes occurring during embryonic development and postnatal growth [17, 18]. So in reality, *Nrf2*<sup>-/-</sup> mice do not develop any spontaneous cancer, but they are more susceptible than wild-type mice to chemical carcinogens [19]. Subsequently, induction of Nrf2 has been recognized as a potential chemopreventive and therapeutic target against carcinogenesis [16, 20, 21]. Contrarily, hyperactive Nrf2 is also reconsidered a potent oncogenic driver with the hallmarks of cancer because of its *bona fide* tumor-promoting effects on carcinogenesis, cancer progression, metastasis, and resistance to therapy [22, 23]. Such opposing roles of Nrf2 in tumor prevention and progression have thereby led us to take account severely of its bidirectional potentials to implicate in cancer treatment. By contrast, Nrf1 is endowed with the unique remarkable features that are distinctive from Nrf2 [6, 24]. This is based on the facts that gene-targeting strategies for knockout of *Nrf1* are employed to create distinct animal models with significant pathological phenotypes [25–30]. Global *Nrf1*<sup>-/-</sup> knockout in mice leads to embryonic lethality at E6.5 to E14.5, resulting from severe oxidative stress damages [25–27]. This presages that loss of Nrf1 cannot be compensated by Nrf2, though both factors can elicit similar overlapping functions in regulating ARE-driven gene expression as confirmed by double knockout (*Nrf1*<sup>-/-</sup>:*Nrf2*<sup>-/-</sup>) [31]. Further, distinct tissue-specific *Nrf1*<sup>-/-</sup> mice are manifested with certain typical pathologies, each of which resembles human nonalcoholic steatohepatitis and hepatoma [28, 29], type 2 diabetes [32], and neurodegenerative diseases [33, 34]. These demonstrate that mouse Nrf1 (and its derivatives) fulfills an indispensable function in regulating critical target genes responsible for maintaining robust physiological development and growth under normal homeostatic conditions. However, the underlying mechanism(s) by which human Nrf1 (and TCF11, that is absent in the mouse) contributes to similar pathophysiological cytoprotection against carcinogenesis remains elusive, as yet.

Our recent work has unraveled that knockout of the human full-length Nrf1 $\alpha$  (including TCF11 and its derivatives, collectively called *Nrf1 $\alpha$* <sup>-/-</sup>) by its *Nfe2l1* gene editing from hepatoma cells leads to aberrant accumulation of Nrf2 [23, 35]. Despite such the activation of Nrf2 and its mediated antioxidant genes, they appear to do nothing to prevent, but conversely promote deterioration of the

*Nrf1* $\alpha^{-/-}$ -derived tumor in the invasion and metastasis [23, 36]. This implies that tumor-promoting effects of Nrf2 are confined competitively by Nrf1, acting as a dominant tumor repressor; this is further corroborated by the evidence showing that no increments in the malignance of liver cancer results from a constitutively active mutant caNrf2 $\Delta^N$  in the presence of Nrf1 [23]. In *Nrf1* $\alpha^{-/-}$  cells, the hyperactive Nrf2 accumulation was determined to result from substantial decreases in protein and mRNA levels of Keap1, GSK-3 $\beta$ , and most of the 26S proteasomal subunits, so that this CNC-bZIP protein degradation is almost abolished. Further mechanistic insights into *Nrf1* $\alpha^{-/-}$ -derived malignance discovered that significantly decreased expression of the tumor repressor PTEN leads to the reversed activation of its downstream AKT oncogenic signaling, as also accompanied by augmented expression of COX-2 and other inflammatory cytokines in *Nrf1* $\alpha^{-/-}$ , but not *Nrf2* $^{-/-}$ , cells [23]. Such being the case, whether the remaining isoforms beyond Nrf1 $\alpha$  contribute to the *Nrf1* $\alpha^{-/-}$  phenotype is unclear.

It is of crucial significance to note the involvement of the epithelial-mesenchymal transition (EMT) in cancer invasion and metastasis, which is modulated by cadherins and  $\alpha$ - and  $\beta$ -catenins (encoded by CTNNA1 and CTNNB1). The latter  $\beta$ -catenin is a versatile player of the Wnt signaling involved in liver development, health, and disease [37–39]. Clearly, the aberrant (and/or mutant) activation of Keap1-Nrf2 and Wnt/ $\beta$ -catenin signaling cascades is a genetic predisposition to hepatocellular carcinoma, in which the CTNNB1 mutation appeared to occur earlier during child liver carcinogenesis, whereas the NFE2L2 mutation was acquired later [40–42]. In  $\beta$ -catenin-driven liver tumors, activation of Nrf2-target antioxidant genes by a mutant  $\beta$ -catenin or another component (Axin1/GSK-3 $\beta$ ) of Wnt signaling also appears to create a protumorigenic environment [43, 44]. Similarly, constitutive activation of both Nrf2-mediated and  $\beta$ -catenin-target genes, along with dysregulation of other critical genes for EMT-related cell shape, cancer invasion, and metastasis behavior, also occurs in *Nrf1* $\alpha^{-/-}$ -derived tumor [23, 36]. As such, a presumable relationship between Nrf1 and  $\beta$ -catenin is not yet established to date.

In this study, we demonstrate that overexpression of Nrf1 enhanced  $\beta$ -catenin ubiquitination for targeting the proteasome-mediated degradation pathway. Conversely, silencing of Nrf1 by its short hairpin RNA (shNrf1) interference caused the accumulation of  $\beta$ -catenin and its translocation into the nucleus. Consequently, a subset of Wnt/ $\beta$ -catenin signaling responsive genes were activated, leading to the putative EMT and related changes in cell shape and behavior. Such silencing of Nrf1 further promoted the mal-growth of human hepatocellular carcinoma, along with malignant invasion and metastasis to the lung and liver in xenograft model mice. Further transcriptomic sequencing identified significant differences in the expression of Wnt/ $\beta$ -catenin-dependent and Wnt/ $\beta$ -catenin-independent responsive genes in shNrf1-expressing cells. Of note, it was identified that  $\beta$ -catenin is not a direct target gene of Nrf1, but the CNC-bZIP factor contributed to the differential or even opposing expression profiles of other critical genes, such as *CDH1*, *Wnt5A*, *Wnt11A*, *FZD10*, *LEF*, *TCF4*, *SMAD4*,

*MMP9*, *PTEN*, *PI3K*, *PDK1*, *JUN*, *ILK*, and *p53*, each of which depends primarily on the positioning of distinct *cis*-regulatory ARE and/or AP1-binding sites within the gene promoter regions. In addition, altered expression profiles of some Wnt/ $\beta$ -catenin signaling proteins were context dependent, as accompanied by the decreased expression of Nrf1 in the clinic human hepatomas with distinct differentiation. Collectively, these corroborate the rationale that Nrf1 acts as a *bona fide* dominant tumor repressor, by intrinsic inhibition of the Wnt/ $\beta$ -catenin and their independent signaling networks involved in cancer development, progression, and malignancy.

## 2. Materials and Methods

**2.1. Cell Lines, Culture, and Transfection.** Four human liver cancer cell lines HepG2, MHCC97H, MHCC97L, and HEK-293T cell lines were maintained in the State Key Laboratory of Cancer Biology, the Fourth Military Medical University. A human immortalized hepatocyte cell line HL7702 and another house liver cancer cell line Hepa1-6 were provided as gifts from the Chinese Academy of Sciences Shanghai Cell Bank (Shanghai, China). All shNC- and shNrf1-expressing cell lines were herein established by a lentivirus-transducing system, which were purified by microfiltration from 293T cells that had been cotransfected with a target vector for shNrf1 or a scrambled shRNA as a negative control (i.e., shNC) along with three packaging vectors, as instructed in a packing kit (GeneCopoeia, Inc., Guangzhou, China). Then, Hepa1-6, HepG2, MHCC97H, and MHCC97L cells were plated in 6-vial plates and transduced with the packaged lentivirus in 8  $\mu$ g/mL of polybrene overnight, before they were allowed for a recovery in a fresh media and continued to incubate for 48–72 h. The positive clones of stably expressing cell lines were selected by 2  $\mu$ g/mL puromycin (Invitrogen) for being used in other experiments.

All experimental cell lines were grown in Dulbecco's Modified Eagle Medium (DMEM; Gibco BRL, Grand Island, NY, USA) containing 10% (*v/v*) fetal bovine serum (FBS; Gibco BRL, Grand Island, NY, USA), supplemented with 100 U/mL penicillin and 100  $\mu$ g/mL streptomycin (Invitrogen, Carlsbad, CA, USA) in a 37°C incubator with 5% CO<sub>2</sub> humidified air. If required, transient transfection of the cells with some indicated plasmids alone or in combination was also performed in the TurboFect Transfection Reagent (Thermo Scientific) or another Lipofectamine<sup>®</sup>3000 Transfection Kit (Invitrogen, Carlsbad, CA, USA), according to the manufacturer's instructions. The cells were then allowed a 24 h recovery from transfection in the fresh medium before being experimented elsewhere. Notably, most of the key reagents and resources used for the following “wet” experiments were listed in Table S1.

**2.2. Real-Time Quantitative PCR.** Experimental cells were subjected to the extraction of total RNAs by using an RNA-simple kit (Tiangen, Beijing, China). Then, 500 ng of total RNA served as a template for the cDNA synthesis by using a RevertAid RT Reverse Transcription Kit (Thermo Fisher



Scientific, USA). The new synthesized cDNA products were further used as the templates of real-time quantitative PCR (qPCR) in the GoTaq<sup>®</sup>qPCR Master Mix (Promega, USA) containing each pair of the indicated primers (with specific nucleotide sequences as listed in Table S1). This reaction was conducted under the following conditions: predegeneration at 95°C for 5 min, followed by 40 cycles of 95°C for 10 s, and 60°C for 30 s. All the qPCR reactions were carried out in at least 3 independent experiments performed in triplicates. The data are shown as fold changes of the mean  $\pm$  SEM ( $n = 3 \times 3$ ), after being normalized by the mRNA level of  $\beta$ -actin, as an internal standard control.

**2.3. Western Blotting of Total Cell Lysates and Its Subcellular Fractions.** Experimental cells were treated with CHX and/or MG132 for distinct lengths of time (as described in details for the relevant figures) before being harvested. The cells were homogenized in RIPA lysis buffer (50 mM Tris, pH 7.5, 150 mM NaCl, 1% NP-40, 0.5% sodium deoxycholate, and 0.1% SDS) containing 2  $\mu$ g/mL protease inhibitors (Roche, Germany). The supernatants of cell lysates were collected before their protein concentrations were determined using a BCA protein assay kit (Pierce Biotechnology, Rockford, IL, USA). Equal amounts (20  $\mu$ g) of protein extracts were then subjected to separation by SDS-PAGE gels containing 8% to 10% polyacrylamide. The resolved proteins were transferred onto PVDF membranes (Millipore). The transferred membranes were blocked by incubation in 5% bovine serum albumin at room temperature for 1 h and then incubated with primary antibody overnight at 4°C. After washing three times, the blots were recognized by the corresponding secondary antibodies for 1 h and also detected by enhanced chemiluminescence with the Odyssey Imaging System (LI-COR Biosciences). The intensity of blots was quantified by the ImageJ software or the Quantity One 4.5.2 software.

Subcellular fractionation of shNrf1- and shNC-expressing cells was conducted according to the previous procedure as described by our group [23, 45]. Then, the cytosolic and nuclear fractions were collected in the sample lysis buffer, followed by Western blotting with the indicated antibodies.

**2.4. The TOPflash Luciferase Reporter Assay to Measure  $\beta$ -Catenin/Tcf-Driven Transcriptional Activity.** Human 293T cells ( $2 \times 10^4$ ) were seeded in each well of a 48-vial plate and allowed for growth to  $\sim$ 70% confluence. The cells were cotransfected with 100 ng of the firefly luciferase reporter called TOPflash (driven by the consensus  $\beta$ -catenin/Tcf4-binding site) or its mutant control plasmid called FOPflash, together with 5 ng of Renilla luciferase reporter (pRL-CMV), plus 10 pmol of indicated small interference RNA targeting for Nrf1 (i.e., siNrf1) or a scrambled negative control RNA (i.e., siNC). At 48 hours after transfection, the cells were subjected to the dual luciferase reporter assay (E1910 from Promega) on a TD-20/20 Luminometer (Turner BioSystems, Sunnyvale, CA), according to the manufacturer's instruction. After the luciferase activity was normalized to the Renilla luciferase values, fold activation of the putative Wnt/ $\beta$ -catenin signaling was quantified by the luminescence ratio of

TOPflash to FOPflash reporters. Subsequently, significant differences in the reporter activity between siNrf1 and siNC were statistically analyzed.

**2.5. Immunoprecipitation with the Ubiquitination Assay.** Human 293T cells ( $5 \times 10^5$ ) grown in 60 mm dishes were cotransfected for 48 h with pcDNA-3 $\times$ HA-Ub (5  $\mu$ g) and pcDNA3.1-V5His-Nrf1 (5  $\mu$ g), along with additional 5  $\mu$ g of either pcDNA-Flag- $\beta$ -catenin or pcDNA-EGFP. The cells were treated with 10  $\mu$ mol/L of MG132 for 4 h before being lysed on ice in the RIPA buffer supplemented with a proteinase inhibitor cocktail (Roche). The cell lysates were pre-cleared with 20  $\mu$ L of protein A/G Agarose (Santa Cruz), before being subjected to immunoprecipitation with 2  $\mu$ g of anti-V5 antibody or mouse IgG (as a blank control), that were incubated overnight at 4°C. The immunoprecipitated beads were further incubated with 30  $\mu$ L of protein A/G Agarose at 4°C for 6 h, before being washed for 5 times in buffer (50 mM Tris, pH 7.5, 10% glycerol, 100 mM NaCl, 0.1% NP-40, 1 mM EDTA, 0.5 mM DTT, and 0.5 mM PMSF). Lastly, 30  $\mu$ L of the loading buffer was added in the washed immunoprecipitates, followed by Western blotting with distinct antibodies against Ub, Flag, and V5 epitopes.

**2.6. Establishment of the Human Tumor Metastasis Model in Nude Mice.** Either shNrf1- or shNC-expressing HepG2 cells ( $4 \times 10^5$  cells in 200  $\mu$ L of serum-free DMEM) were injected through the tail veins of nude mice (of 6-week-old male, from the FMMU Laboratory Animal Center) that had been divided into two groups. At 6 weeks after cell inoculation, these animals were sacrificed and then subjected to the pathological and histochemical examinations. The volume of metastatic tumors in the murine lung and liver were calculated by the formula  $\pi/6 \times \text{length} \times \text{width}^2$ .

**2.7. The Subcutaneous Tumor Model of Human Xenografts in Nude Mice.** Mouse xenograft models were also made by subcutaneous heterotransplantation of the human hepatoma HepG2 cell lines expressing shNrf1 or shNC into nude mice (as described above). Equal amounts of the indicated cells ( $1 \times 10^7$  cells that had grown in the exponential phase) were sufficiently suspended in 200  $\mu$ L of serum-free DMEM and then inoculated subcutaneously into the right upper back region of male nude mice (BALB/C nu/nu, 6 weeks old, 16 g, from HFK Bioscience, Beijing, China) at a single site. The procedure of injection into all the experimental mice was completed within 30 min, and the subsequent formation of the subcutaneous tumor xenografts was observed. Once the tumor xenografts emerged, the sizes of these ongoing tumors were successively measured once every two days, until the 42<sup>nd</sup> day when these mice were sacrificed and their transplanted tumors were excised. Thereafter, distinct sizes of those growing tumors were also calculated by a standard formula (i.e.,  $V = ab^2/2$ ) and are shown graphically ( $n = 7$  per group). The tumor tissues were also subjected to the pathohistological examination and Western blotting.

Notably, all the relevant animal experiments in this study were indeed conducted according to the valid ethical regulations that have been approved. All mice were maintained

under standard animal housing conditions with a 12 h dark cycle and allowed access ad libitum to sterilized water and diet. All relevant studies were carried out on 6-week-old male mice (with the license No. PIL60/13167) in accordance with the United Kingdom Animal (Scientific Procedures) Act (1986) and the guidelines of the Animal Care and Use Committees of Chongqing University and the Third Military Medical University, both of which had been subjected to the local ethical review (in China). All the related experimental protocols had been approved by the University Laboratory Animal Welfare and Ethics Committee (with two institutional licenses SCXK-PLA-20120011 and SYXK-PLA-20120031).

**2.8. Tumor Pathohistological Examination with Immunohistochemistry.** Murine subcutaneous xenograft tumors derived from shNrf1- or shNC-expressing human hepatoma cells, along with several human liver cancer and adjacent tissues (obtained from the Pathological Tissue Bank of Hospital affiliated to the Third Military Medical University), were fixed with paraformaldehyde (4%) and embedded in paraffin before the sections of 5  $\mu$ m slices were prepared. Firstly, the sections were dewaxed in the pure xylene twice (each for 5 min) and then washed in 100% ethanol twice (each for 5 min) to eliminate xylene, followed by rehydration in a series of gradient concentrations of ethanol with distilled water. Subsequently, they were stained with the routine hematoxylin and eosin (H&E) and visualized by microscopy. As for immunohistochemical staining, after the indicated tissue samples were dewaxed and rehydrated, they were treated with 3% hydrogen peroxide before being boiled in the microwave for 15 min in a citrate buffer (pH 6.0) to retrieve the putative antigen. The slides were blocked with 1% bovine serum albumin for 60 min and then incubated at 4°C overnight with the primary antibodies against Nrf1 (saved in our group) and TCF4 (both at a dilution of 1:50). Thereafter, the primary antibody-stained slides were reincubated with a biotin-conjugated secondary antibody for 60 min at room temperature, before being visualized by the peroxidase-conjugated biotin-streptavidin complex (Boster, Wuhan, China). In similar experimental settings, the negative staining controls were also set up by replacing the primary antibody with the normal nonimmune serum diluted in PBS. The resultant images were acquired under a light microscope (Leica DMIRB, Leica, Germany) equipped with a DC350F digital camera.

Further examination of the tumor metastatic liver and lung tissues was performed as described above. In brief, the tissues were fixed in 10% neutral buffered formalin and embedded in paraffin. The sections were subjected to routine pathohistological examination by H&E staining. The immunohistochemical staining was also conducted by incubation of indicated sections with distinct primary antibodies against human Nrf1 (from Cell Signaling Technology, Inc.),  $\beta$ -catenin, and Cyclin D1 (both obtained from Epitomics, Hangzhou, China), each of which was diluted at 1:100, and with the secondary antibody against rabbit IgG, which had been conjugated with horseradish peroxidase. The stained sections were developed with a

3,3'-diaminobenzidine kit (Boster Biotech, Wuhan, China), according to the manufacturer's instruction.

**2.9. Distinct Enhancer-Driven Luciferase Reporter Assays.** Equal numbers ( $5 \times 10^4$ ) of experimental cells were grown in 24-well plates. After reaching 80% confluence, the cells were cotransfected with each of those indicated firefly luciferase plasmids (containing distinct target gene promoter regions, their consensus regulatory elements such as ARE, AP1-, and  $\beta$ -catenin/TCF-binding sites, their mutants) or an empty plasmid with no enhancer to be encompassed, along with a Renilla luciferase plasmid and an expression construct for Nrf1,  $\beta$ -catenin, or Ub alone or in combination, in the Lipofectamine-3000 mixture. After transfection for 24 h, the cells were harvested by adding 200  $\mu$ L of lysis buffer in each well. The cell lysates were subjected to the reporter assay by the dual-luciferase reporter system. Of note, the Renilla luciferase expressed by the pRL-TK plasmid served as an internal control for transfection efficiency. The luciferase activity was measured by the dual-luciferase reporter assay system (E1910, Promega, Madison, WI, USA). The resulting data were normalized and calculated as a fold change (mean  $\pm$  SEM) relative to the activity of the control group (at a given value of 1.0). All the data presented in this study represent at least three independent experiments undertaken on separate occasions which were each performed in triplicate. Significant differences in the transcriptional activity were determined by statistical analysis. For a detailed description of the  $\beta$ -catenin/Tcf-driven TOPflash reporter and its mutant FOPflash in the luciferase assays, please see the relevant supplementary information. In addition, all the core sequences of ARE and AP1-binding sites were shown in Table S1.

**2.10. Analysis of the Genome-Wide RNA-Sequencing.** After total RNAs were extracted by using an RNAsimple kit (Tiangen, Beijing, China), the integrity of purified RNAs was also validated by an Agilent Bioanalyzer 2100 system (Agilent Technologies, Santa Clara, CA). For each sample, equal amounts of total RNAs were collected from three independent experiments and pooled together for RNA-sequencing (RNA-Seq). Subsequently, RNA-Seq was carried out by the Beijing Genomics Institute (BGI, Shenzhen, China) on an Illumina HiSeq 2000 sequencing system (Illumina, San Diego, CA) after the sample library products are ready for sequencing. After the RNA-Seq quality was examined by removing the "dirty" raw reads, which contain low-quality reads and/or adaptor sequences, the clean reads were generated and stored as the FASTQ format. Thereafter, the clean reads were mapped to the reference of the human genome (GRCh37/hg19 from UCSC database) by using SOAP2, before distinct gene expression levels were calculated by using the RPKM (reads per kilobase of feature per million mapped reads) method. Notably, those differential expressed genes (DEGs) were further identified by the Poisson distribution model method (PoissonDis), which was developed referring to "the significance of digital gene expression profiles" by BGI. Both  $FDR \leq 0.001$  and the absolute value of  $\log_2$  (fold change)  $\geq 1$  were herein taken as the threshold, in order to

be identified as each of DEGs. The pathway enrichment analysis was also performed by using the online KEGG database (<https://www.kegg.jp/>). In addition, the putative interaction networks of Nrf1-related genes involved in carcinogenesis, migration, metastasis, and metabolism were annotated with the sequencing results by the Cytoscape software.

**2.11. Statistical Analysis.** The “wet” experimental data provided in this study were represented as a fold change (mean  $\pm$  SD), each of which represents at least 3 independent experiments that were each performed in triplicate. Significant differences were statistically determined using the Student *t*-test, Fisher exact test, and multiple analysis of variations (MANOVA), as appropriate. The resulting value of  $p < 0.05$  was considered a significant difference. Furthermore, another statistical determination of the “dry” sequencing analysis was also carried out as described by Wang et al. [46].

### 3. Results

**3.1. Establishment of Stable shNrf1-Expressing Hepatoma Cell Lines.** For this end, we firstly investigated differential abundances of Nrf1 $\alpha$ /TCF11 and derivative isoforms between 140 kDa and 100 kDa in a noncancerous human liver HL7702 and other four human hepatoma-derived cell lines (Figure 1(a)). Upon exposure of all five cell lines to proteasomal inhibitor MG132, most of the Nrf1 $\alpha$ /TCF11-derived proteoforms were obviously increased (Figure 1(a)). Conversely, significant knockdown of Nrf1 by shNrf1 (interfering its specific mRNA sequence encoding amino acids 397-406) was identified by real-time quantitative PCR (RT-qPCR) analysis of HepG2, MHCC97H, and MHCC97L cell lines (Figure 1(b)). Accordingly, both basal and MG132-stimulated abundances of NQO1 (containing an ARE enhancer within the gene promoter region) were strikingly suppressed as accompanied by silencing of Nrf1 (Figure 1(c)). Most of the Nrf1 $\alpha$ /TCF11-derived proteoforms were substantially diminished or abolished by shNrf1, particularly in the presence of MG132, and such downward trends of Nrf1 and NQO1 were also corroborated by further quantitative analysis (Figures S1 and S2). On this basis, a stable shNrf1-expressing HepG2 cell line was established by a lentivirus-mediated shRNA transduction system, and determined by transcriptomic sequencing, to yield a considerably lower level of *Nrf1* mRNA than that obtained from scrambled shNC control (Figure 1(d)). The reliability of shNrf1 with workable efficacy was further validated by the profiling of the *Nrf1* gene expression in shNrf1- and shNC-expressing HepG2 cell lines. The results unraveled that 10 of at least 12 transcripts of *Nrf1* mRNAs (enabling the translation of distinct lengths of polypeptides) were mostly silenced by shNrf1 (i.e., ~75%, as deciphered in Figures 1(e) and S2B, S2C).

**3.2. Knockdown of Nrf1 Leads to Phenotypic Changes in the shNrf1-Expressing Cell Shape and Behavior.** Herein, we noticed obvious phenotypic changes in the morphology of shNrf1-expressing HepG2 cells (as shown in Figure 1(f),

right panel). These Nrf1-deficient cells are sparsely scattered and displayed the slender spindle-like shapes with some long slim pseudopods being protruded. Such obvious phenotypic changes are fitted as consistent with characteristics of the mesenchymal cell morphology, termed by Morriss and Solursh [47]. However, no changes in the morphology of shNC-expressing HepG2 cells were compared with the characteristics of the non-lentivirus-transfected cells; they are oval-shaped with a few of short hornlike projections and also huddled together acting as a lump of the paving stones (Figure 1(f), left-middle panels). Such morphological differences between shNrf1-expressing and control cell lines convincingly demonstrate that knockdown of Nrf1 results in the EMT process of hepatoma cells.

To investigate an effect of Nrf1 on the cancer migratory behavior, we performed the *in vitro* scratch wound-healing assays of distinct three pairs of hepatoma cell lines expressing shNrf1 or shNC, respectively. As anticipated, the results revealed that migration of those shNrf1-expressing hepatoma cells, particularly derived from HepG2 and MHCC97H, was markedly enhanced by knockdown of Nrf1 (Figure 1(g) and S3A). Furtherly, the Matrigel invasion assay showed that the number of putative invading cells was strikingly incremented by silencing of Nrf1 in all three shNrf1-expressing cell lines when compared with the counterpart shNC-expressing controls (Figure 1(h) and S3B). These collective results presage that migration and invasion of human hepatoma cells are promoted by knockdown of Nrf1.

**3.3. Silencing of Nrf1 Causes Malgrowth of shNrf1-Expressing HepG2 with the Shorten G1 Phase of Cell Cycles.** The cell viability was determined for whether the growth of hepatoma was affected by knockdown of Nrf1. The results showed that the growth of shNrf1-expressing hepG2 cells was accelerated at a certain rate, by comparison of the shNC-expressing control cells (Figure S4A, left panel). However, almost no effects of Nrf1 knockdown on the growth of MHCC97H and MHCC97L were also observed (Figure S4A, right panel).

The colony formation assay of hepatoma cells grown *in vitro* unraveled a ~40% increase in the number of colonies of the shNrf1-expressing HepG2 cells, relative to the shNC-expressing control value (Figure 1(i)). Rather, almost no effects of such shNrf1-expressing lentivirus on the colony formation of MHCC97H and MHCC97L cells were observed (Figure S4B, S4C). Further examinations by flow cytometry discovered that the G1 phase of the shNrf1-expressing HepG2 cell cycles was significantly shortened by ~16% of shNC controls, while the G2/M phase was relatively extended by 2-fold changes relative to the shNC control, but their S phases were unaffected by silencing of Nrf1 (Figure S4D1). Contrarily, almost no changes in the G1 phase of MHCC97H and MHCC97L cell cycles were examined, by comparison of shNrf1 and shNC silencing, but the S phases were modestly shortened, as accompanied by the relative longer G2/M phases (Figure S4D2, S4D3). In addition, only early apoptosis of shNrf1-expressing HepG2 cells was increased, when compared with shNC controls (Figure S4E1), but no changes in all other cases were



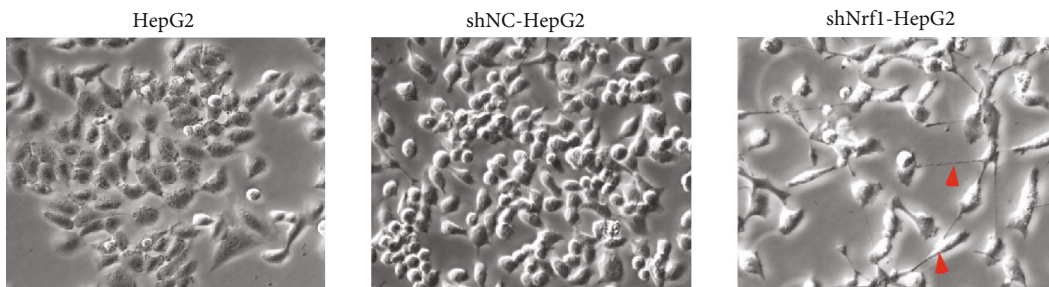
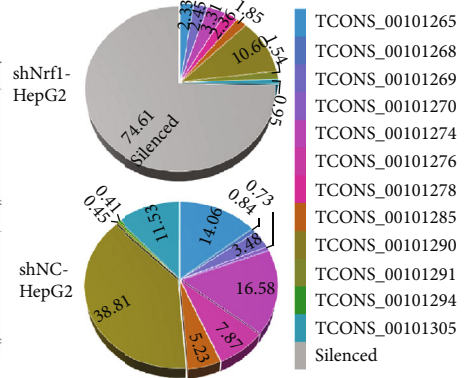
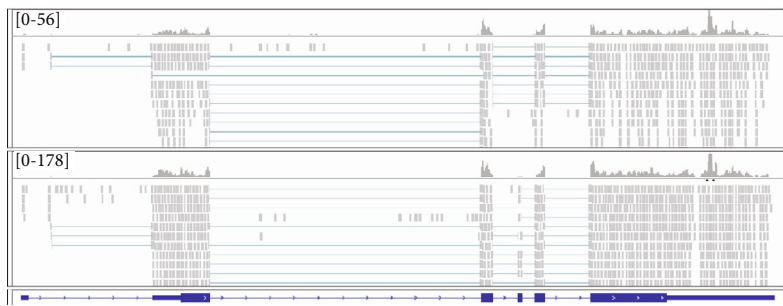
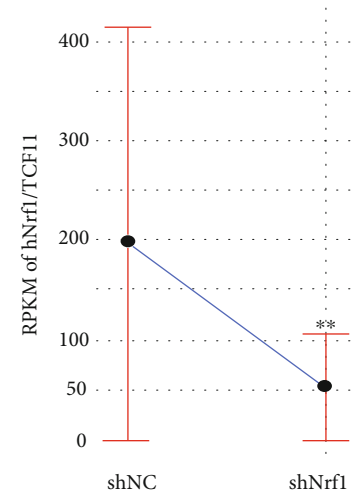
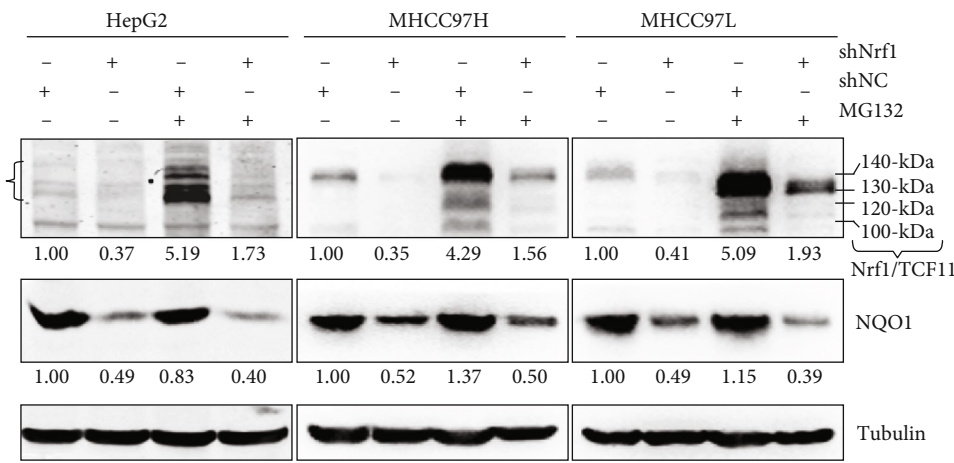
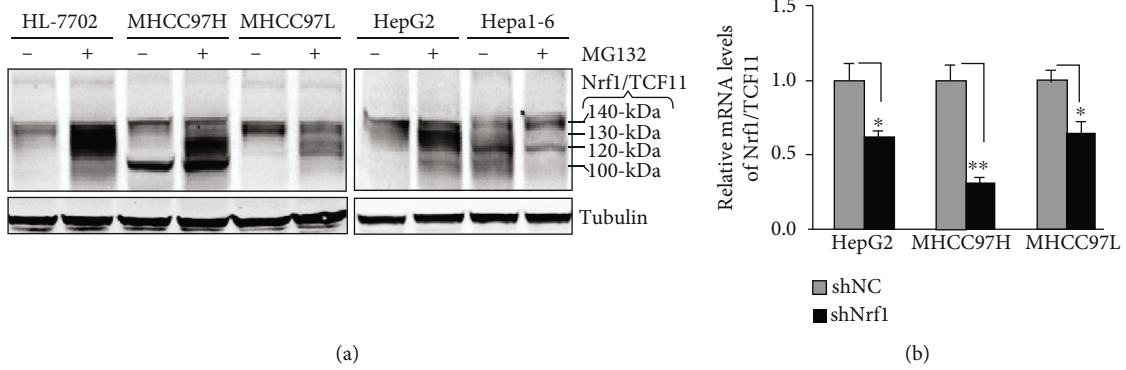


FIGURE 1: Continued.

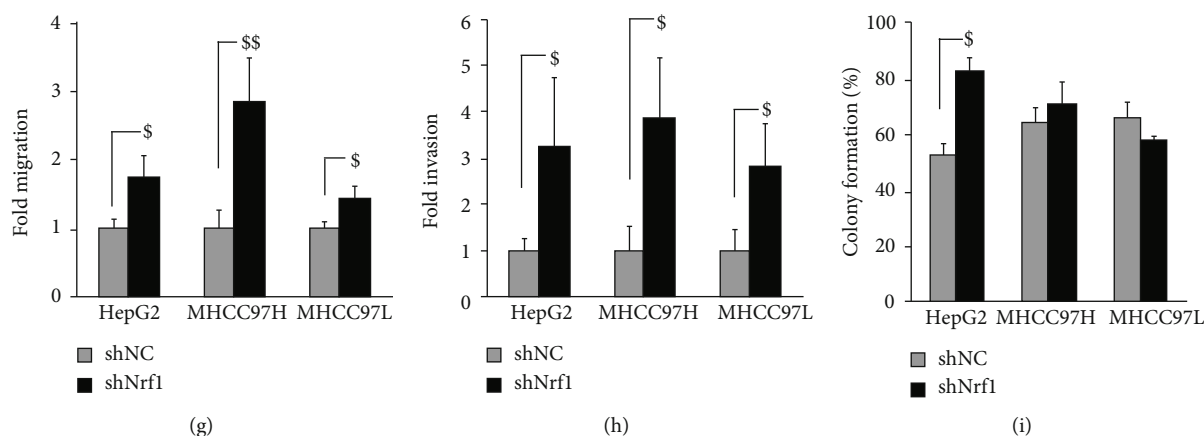


FIGURE 1: Identification of stably expressing shNrf1 hepatoma cell lines with altered shapes and malignant behaviors. (a) Western blotting of hNrf1/TCF11 expression in a noncancerous HL-7702 and four hepatocarcinoma cell lines that were treated with 10  $\mu\text{mol/L}$  of MG132 (+) or vehicle controls (-, DMSO) for 4 h. (b) Real-time qPCR analysis of the lentiviral-mediated knockdown of hNrf1/TCF11 by its short hairpin RNA (shNrf1) interference in three examined cell lines. The scrambled short hairpin RNA sequence serves as an internal negative control (shNC). The data are shown as mean  $\pm$  SEM ( $n = 3 \times 3$ ), after significant decreases ( $*p < 0.05$ ;  $**p < 0.01$ ) of shNrf1 relative to the shNC values were determined. (c) Western blotting of Nrf1/TCF11 and its target NQO1 in three pairs of shNrf1- and shNC-expressing cell lines that were treated with 10  $\mu\text{mol/L}$  of MG132 (+) or vehicle control (-, DMSO) for 4 h. The intensity of the above immunoblots was quantified by the Quantity One 4.5.2 software and are shown graphically (in Figure S1). (d) Identification by transcriptomic sequencing of the *hNrf1/TCF11* gene expression profiles of shNrf1- and shNC-silenced HepG2 cells. (e) The comparison of sequence reads (left panels) that were distributed to the genomic reference of the concrete and complete expression levels of the single *hNrf1/TCF11* gene in the two samples of shNrf1- and shNC-HepG2 cell lines by using the IGV (Integrative Genomics Viewer) tool. A relative proportion of all the examined individual transcript isoforms of *hNrf1/TCF11* was illustrated by each of the pie charts (right panels). (f) The morphological changes in the shape of HepG2 cells that had been transduced by a lentivirus containing shNrf1 or shNC, as well as its progenitor cells, were photographed in a low-power field (200x). (g) Fold migration and (h) invasion of shNrf1-expressing cells represent the mean  $\pm$  SD of three independent experiments in triplicates ( $n = 3 \times 3$ , in Figure S3). Significant increases ( $^{\$}p < 0.05$ ;  $^{\$\$}p < 0.01$ ) were determined by one-way ANOVA analysis, relative to shNC controls. (i) Cell colonies on the plates were stained with 1% crystal violet reagent before being counted (Figure S4C). The data were calculated as a fold change (mean  $\pm$  SD,  $n = 3$ ;  $^{\$}p < 0.05$ ) of the shNrf1-derived clone formation, relative to the shNC controls.

examined by fluorescence-activated cell sorting (Figure S4E2, S4E3). Together, these imply that silencing of Nrf1 leads to the malgrowth of shNrf1-expressing HepG2 cells, possibly resulting from the shortened G1 phase of cell cycles.

**3.4. Activation of  $\beta$ -Catenin and Other Critical Genes for the Malignant Behavior of Nrf1-Silenced Cells.** Since the migration and invasion of the tumor are pinpointed to two major characteristics of cancer malignancy [48], we here examine the expression profiles of several putative genes involved in migration and invasion. As anticipated, it was found that when compared with shNC controls, shNrf1-expressing HepG2 cells yielded a substantial augment in the mRNA expression of genes encoding matrix metalloproteinase-2 (MMP2) and MMP9 (Figure 2(a)). Such activation of MMPs leads to potential proteolytic degradation of the extracellular matrix, thereby allowing cancer cells to break through the *in situ* matrix confinements for migration and invasion. Meanwhile, the matrix basement membrane that surrounds epithelial cells was also slackened by significant downexpression of *CDH1* (encoding E-cadherin, as a specific marker required for the cell adhesion) in the Nrf1-silencing HepG2 cells (Figure 2(a)). Similarly, opposite changes in the protein expression levels of E-cadherin and MMP9 were further determined by Western blotting of shNrf1-expressing cell

lines, when compared to equivalent controls from shNC-expressing cells (Figures 2(b) and 2(c)).

Interestingly, a significant increased abundance of vimentin was also detected in all the Nrf1-silencing cell lines, by comparison to the corresponding shNC controls (Figures 2(b), B3 and 2(c) C3). Here, it should be noted that vimentin serves as a mesenchymal marker, due to the deformability of the mesenchymal stem cells that depend on vimentin [49], because it can maintain cell shape and integrity and stabilizes cytoskeletal interactions. Together, these abovedescribed results indicate that knock-down of Nrf1 leads to the putative EMT shaping in a cell-autonomous manner, whereby it plays an important role in cell migration and invasion, as deciphered by Kalluri and Weinberg [50].

It is plausible that the E-cadherin can also exert as a tumor suppressor to prevent cells from growing, dividing, and moving in a rapidly uncontrolled way. Such functionality of the E-cadherin in controlling cell maturation and movement is attributable to its predominant interactions with p120-catenin proteins, in order to regulate the activity of cognate genes [37]. Among them,  $\beta$ -catenin is a key component of the Wnt signaling that is important for normal development, growth, and disease (e.g., cancer) [38, 51, 52]. When required for biological cues,  $\beta$ -catenin is allowed for release from physical interaction with E-cadherin to translocate the



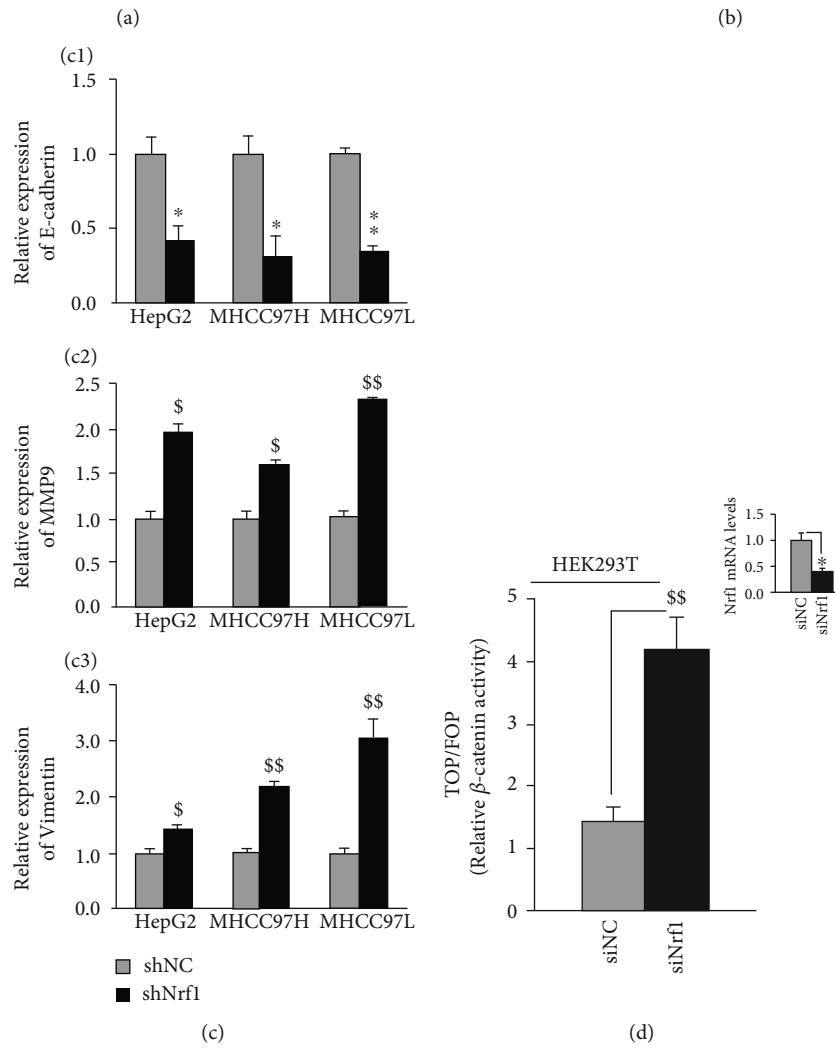
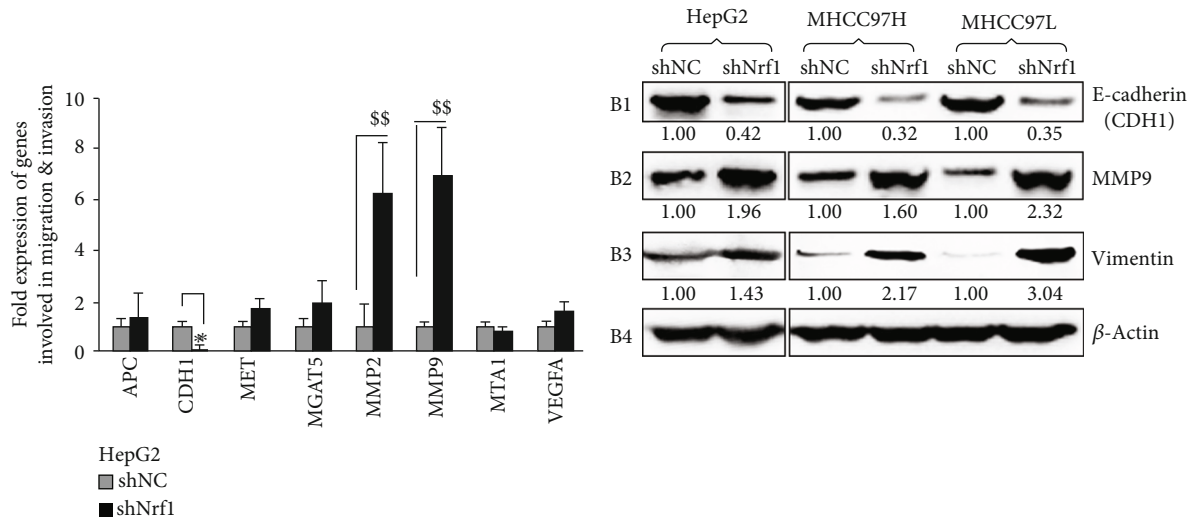


FIGURE 2: Continued.

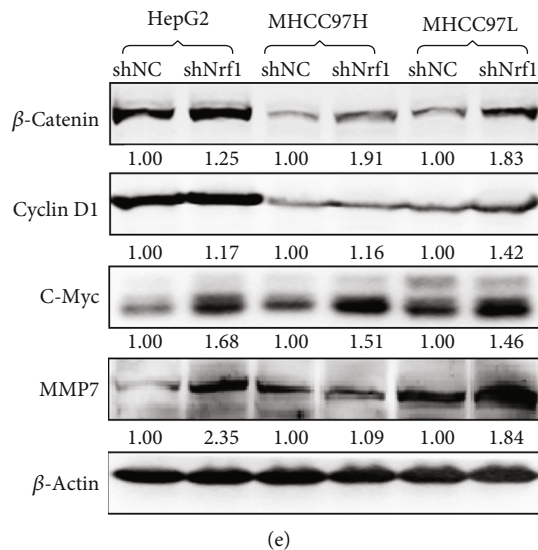


FIGURE 2: Activation of  $\beta$ -catenin signaling pathway by knockdown of Nrf1 in hepatoma cells. (a) Real-time qPCR analysis of differential expression of those genes that are involved in migration and invasion of shNrf1- or shNC-transduced HepG2 cells. The data were shown as the mean  $\pm$  SEM ( $n = 3 \times 3$ ). Significant increases ( $^{ss}p < 0.01$ ) or decreases ( $^{*}p < 0.05$ ) were statistically calculated by comparison with the shNC controls. (b, c) Abundances of E-cadherin, vimentin, and MMP9 were detected by Western blotting with the indicated antibodies (b). The intensity of their immunoblots was quantified by the Quantity One 4.5.2 software (c). The data are representative of three independent experiments and also graphically shown as the mean  $\pm$  SD ( $n = 3$ ). Significant increases ( $^{s}p < 0.05$ ;  $^{ss}p < 0.01$ ) were caused by silencing of Nrf1, relative to the shNC control values. (d) The relative  $\beta$ -catenin/TCF-mediated luciferase activity was determined by measuring HEK293T cells that had been cotransfected with either TOPflash (wild-type) or FOPflash (a mutant that serves as a background control) along with specific siRNAs targeting to Nrf1 (siNrf1). In addition, knockdown of Nrf1 was validated herein. The data were shown as the mean  $\pm$  SEM ( $n = 3 \times 3$ ). Knockdown of Nrf1 caused a significant increase of  $\beta$ -catenin activity ( $^{ss}p < 0.01$ ) and another significant decrease of Nrf1 ( $^{*}p < 0.05$ ), which were statistically calculated by comparison with the control values obtained from siNC-transfected cells. (e) Basal abundances of  $\beta$ -catenin, Cyclin D1, c-Myc, and MMP7 in distinct pairs of the shNrf1- and shNC-derived hepatoma cell lines were visualized by Western blotting with their respective antibodies. Then, the intensity of their immunoblots was determined and shown on each of the bottoms.

nucleus and acts as a coactivator to bind one of its partner transcription factors LEF or TCF (including TCF1, TCF3, or TCF4). The resulting  $\beta$ -catenin/TCF complex can enable target genes to be transcriptionally activated upon induction of Wnt signaling. The TCF-binding motif (5'-AGATCA AAGG-3') is widely used for the Wnt/TCF reporter, such as pTOPflash [53]. Herein, similar TOP/FOPflash assay revealed that the  $\beta$ -catenin/TCF transactivity was significantly augmented by knockdown of Nrf1 (Figure 2(d)). The protein expression of  $\beta$ -catenin was also obviously enhanced in all the Nrf1-silenced cell lines (Figure 2(e)). This was accompanied by elevated expression of those  $\beta$ -catenin/TCF-target genes encoding Cyclin D1, c-Myc, and MMP7. Therefore, these demonstrate that stable knockdown of Nrf1 results in constitutive activation of the Wnt/ $\beta$ -catenin signaling pathway triggered in all the shNrf1-expressing cells.

**3.5. Malgrowth of the Human Nrf1-Silenced Tumor with Metastasis to the Lung and Liver in Xenograft Mice Is Relevant to  $\beta$ -Catenin Signaling Activation.** To determine the contribution of Nrf1 knockdown to distant metastasis of cancer *in vivo*, here, we injected the human shNrf1- or shNC-expressing HepG2 cells ( $2 \times 10^6$  in a solution of 200  $\mu$ L) into nude mice through their tail veins. Then, six

weeks later, these mice were sacrificed and dissected. The anatomical observations showed that all the mice became the human hepatoma xenograft bearers in their lungs and livers (Figures 3(a) and 3(c)). A lot of many bigger metastatic tumor nodules were presented in the shNrf1-silenced animals, whereas only a very few smaller metastatic tumors emerged in the shNC control mice. Further, the histochemical and immunocytochemical staining unraveled that  $\beta$ -catenin and Cyclin D1 were highly expressed in the shNrf1-silenced tissue sections of the murine lung and liver, by comparison with the shNC controls (Figures 3(b) and 3(d)).

To further examine *in vivo* malgrowth of human hepatoma and distant migration, the shNrf1- or shNC-expressing HepG2 cells ( $1 \times 10^7/200 \mu$ L) were inoculated subcutaneously into nude mice. The incubation period of tumorigenesis before the injected *in situ* emergences of visible tumor xenografts derived from shNrf1-silenced cells were strikingly shortened by 40% of the control values obtained from shNC cells (Figures 3(e) and 3(f)). Thereafter, clear sizeable increments in the growth of the human hepatoma xenografts were shown graphically (Figure 3(f)); a steep S-curve represented the rapid rising malgrowth of the shNrf1-derived tumors, by contrast with an shNC-derived tumor only displaying a smooth gradual growth curve. Of note, all the Nrf1-silenced hepatoma xenograft mice, but

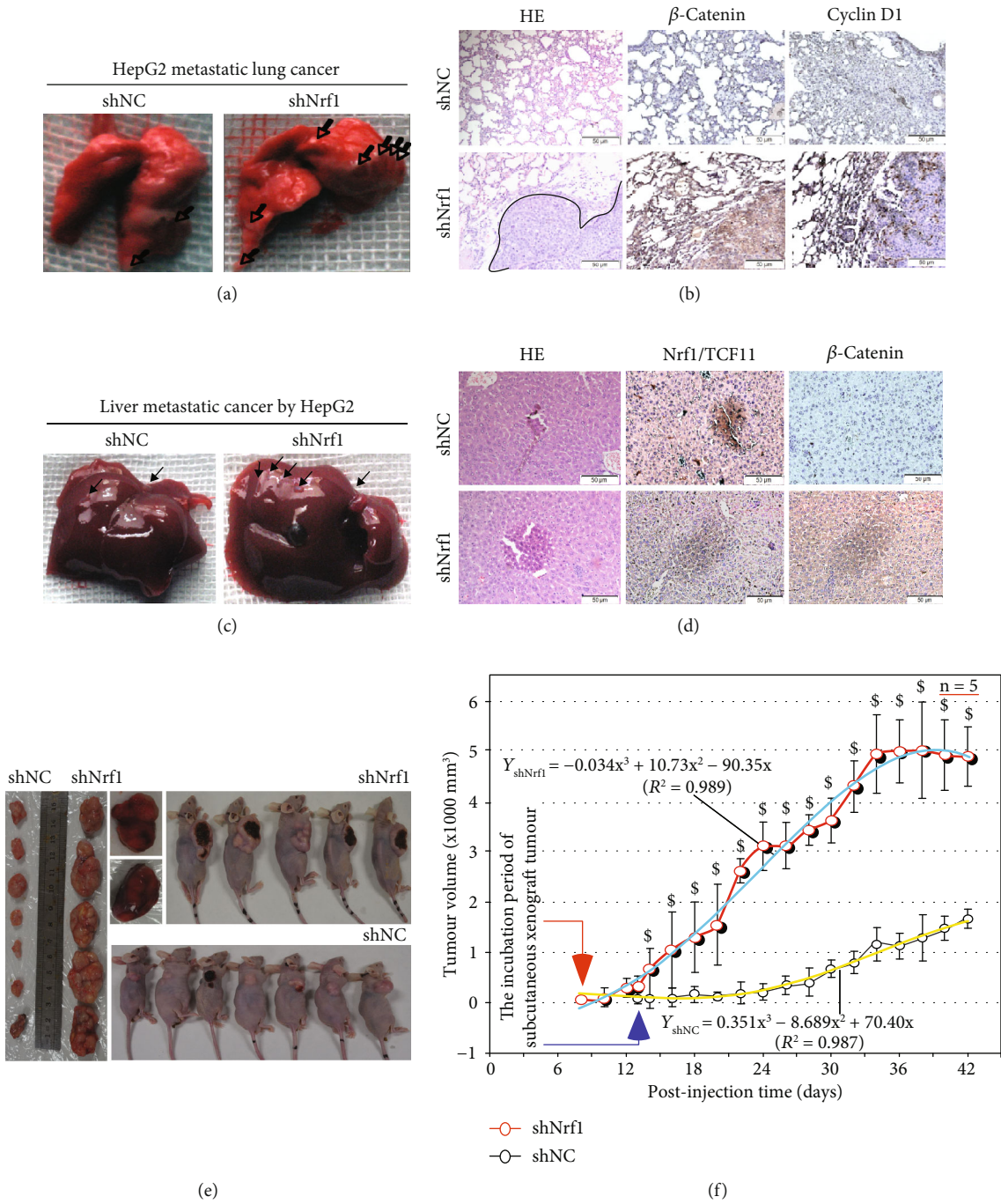


FIGURE 3: Continued.



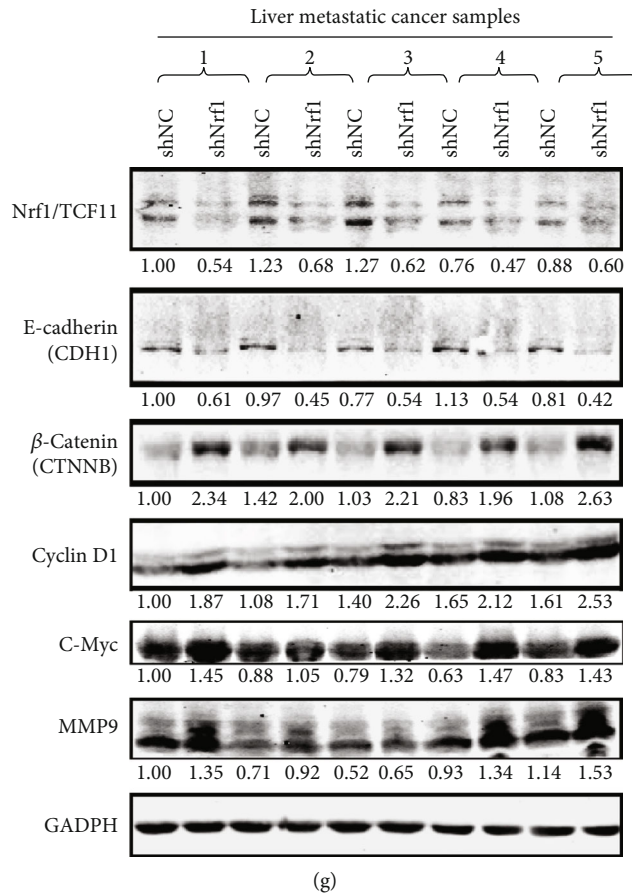


FIGURE 3: Significant enhancements in the *in vivo* malgrowth of Nrf1-silenced hepatoma cells and metastatic potentials. (a) The lung metastatic tumors in the nude mice that had been intravenously injected with shNrf1- or shNC-expressing HepG2 cells in a 200  $\mu$ L solution. Some metastatic tumors were arrowed. (b) The lung metastatic tumor tissues were stained with the hematoxylin-eosin (HE) method and also subjected to immunohistochemistry with antibodies against  $\beta$ -catenin and Cyclin D1. The resulting images were acquired (200x). (c) The liver metastatic tumors from the above xenograft mice. Some metastatic tumors were indicated by arrows. (d) Similar HE staining of the liver metastatic tumor tissues was also performed, along with immunohistochemical staining with antibodies against Nrf1 and  $\beta$ -catenin. The resulting images were shown herein (200x). (e) Two distinctive groups of the animal xenograft tumors in nude mice that had been subcutaneously inoculated with shNrf1- and shNC-expressing HepG2 cells. Of note, the shNC group seems similar to those of the wild-type control group (in the parallel experiments as reported by our research team [36]). (f) Different growth curves of the above mouse subcutaneous xenograft tumors. After the subcutaneous tumor emerged in each of the mice that had been inoculated with shNrf1- and shNC-expressing hepatoma cells, they were then measured in size every two days, before being sacrificed on the 42<sup>nd</sup> day. The data are shown as mean  $\pm$  SD ( $n = 7$  per group, but with an exception that two shNrf1-bearing mice died of cancer cachexia syndrome on the 40<sup>th</sup> day). Significant increases of shNrf1-derived tumors ( $^*p < 0.05$ ) were calculated by comparison with the shNC controls. (g) Distinct expression abundances of Nrf1, E-cadherin,  $\beta$ -catenin, Cyclin D1, c-Myc, and MMP9 in the liver metastatic xenograft tumors were detected by Western blotting with their respective antibodies. The intensity of their immunoblots was quantified as shown on each of the bottoms.

not the shNC control mice, suffered from a severe syndrome resembling the human cancer cachexia, as described previously [36]. The occurrence of the cancer cachexia syndrome was attributable to hepatic metastasis, leading to the early death of two mice before being designedly sacrificed (Figure 3(e), upper-middle panels). Yet, no similar pathological changes were observed in the shNC control mice.

These metastatic tumors were also subjected to the aforementioned histopathological staining (Figures 3(b) and 3(d)) and the following Western blotting analysis. The results unraveled that silencing of Nrf1 led to significant decreases of E-cadherin in the hepatic intratumor tissues of shNrf1-expressing hepatoma xenograft mice (Figure 3(g)). Interest-

ingly, this was also accompanied by varying extents of increases in the intratumor expression of  $\beta$ -catenin, Cyclin D1, c-Myc, and MMP9. Together, these demonstrate that knockdown of Nrf1 leads to constitutive activation of  $\beta$ -catenin signaling pathway, and therefore results in a significant enhancement in the *in vivo* malgrowth of hepatoma and its malignant metastatic potentials.

**3.6. Knockdown of Nrf1 Causes  $\beta$ -Catenin Activation and Translocation to Regulate the Nuclear Target Genes.** To clarify the mechanism underlying the constitutive activation of  $\beta$ -catenin by knockdown of Nrf1, here, we firstly scrutinized the cycloheximide (CHX) chase analysis of both protein

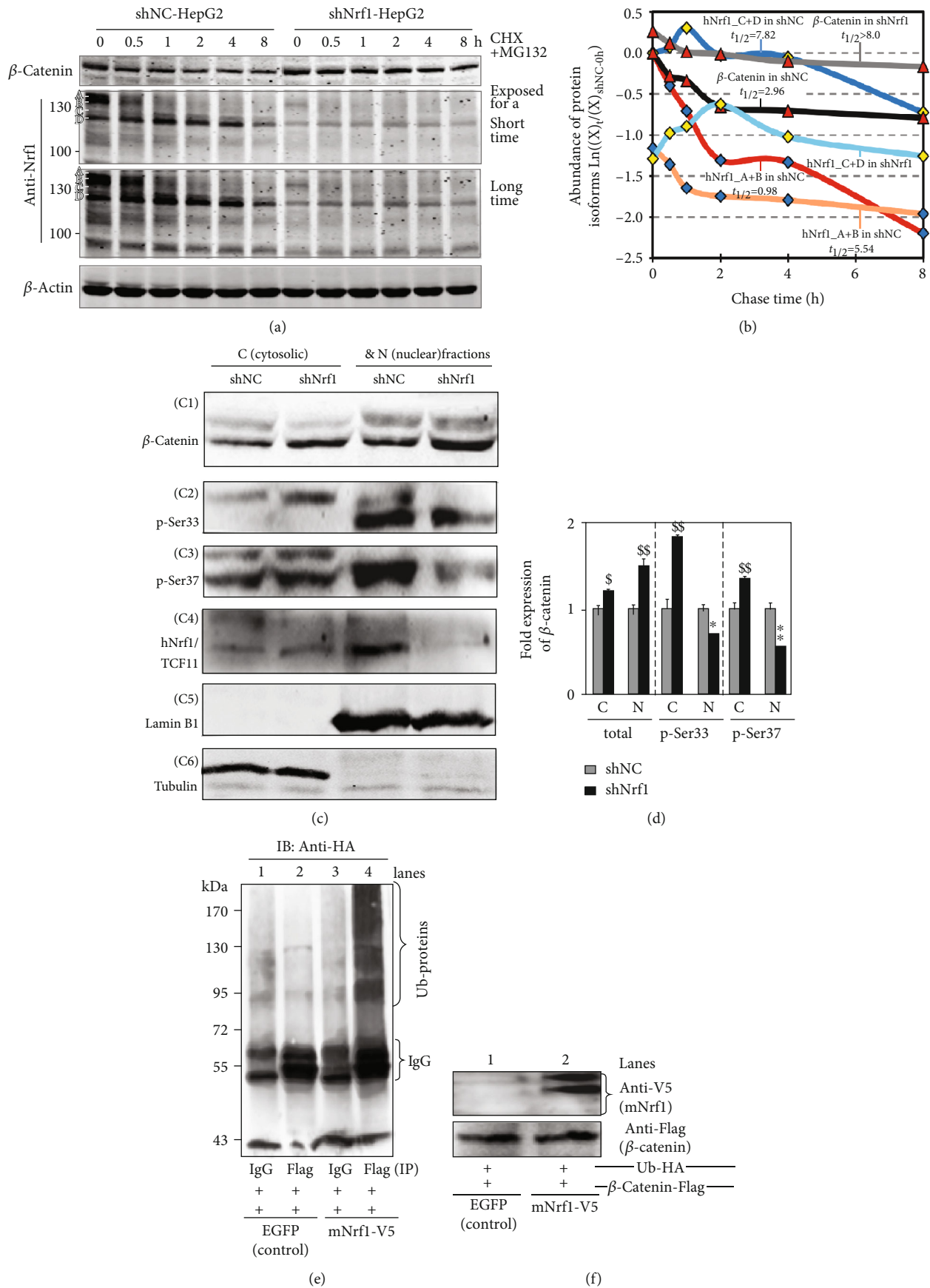


FIGURE 4: Continued.

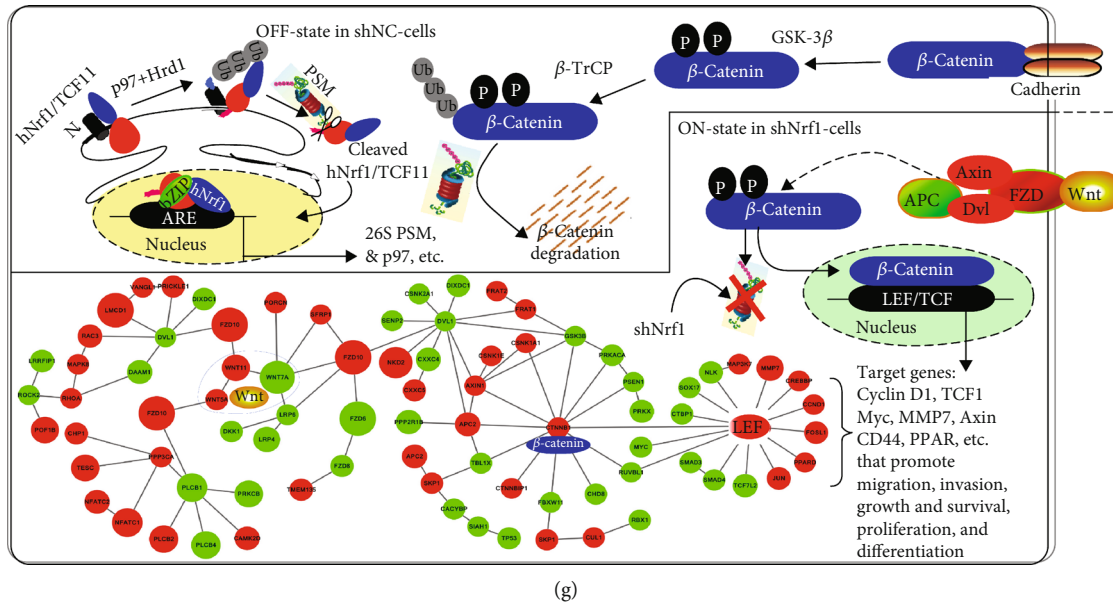


FIGURE 4: Significant increases in the  $\beta$ -catenin stability and nuclear translocation to regulate target genes in Nrf1-silenced cells. (a) Experimental shNC- and shNrf1-expressing HepG2 cells had been cotreated with CHX (100  $\mu$ g/mL) and MG132 (5  $\mu$ mol/L) for indicated lengths of time before being harvested. Both  $\beta$ -catenin and Nrf1 expression levels were detected by Western blotting, and the resulting immunoblots were quantified by the Quantity One 4.5.2 software. (b) These data are shown graphically. Of note,  $(X)_t/(X)_{shNC-0h}$  represents a relative amount of the indicated proteins measured at the indicated “t” time points, that was also normalized to the shNC control value obtained at the 0 h point. (c) Both the cytosolic (i.e., C) and nuclear (i.e., N) fractions of the total  $\beta$ -catenin and its phosphorylated proteins were obtained from shNrf1- or shNC-expressing HepG2 cells and subjected to visualization by Western blotting with indicated antibodies. (d) The intensity of all the blots representing total  $\beta$ -catenin and its phosphorylated proteins was quantified by densitometry and normalized to the control values measured from shNC-transduced cells. The data are shown as mean  $\pm$  SD ( $n = 3$ ) representing at least three independent experiments undertaken on separate occasions. Significant increases ( $^s p < 0.05$ ;  $^{ss} p < 0.01$ ) and decreases ( $^* p < 0.05$ ;  $^{**} p < 0.01$ ) of Nrf1-silenced hepatoma cells were determined by comparison to the equivalent shNC values. (e, f) Promotion of  $\beta$ -catenin ubiquitination by overexpression of mouse Nrf1 (i.e., mNrf1). Experimental 293T cells were cotransfected with expression constructs for mNrf1 (with the C-terminal V5 epitope) and  $\beta$ -catenin (tagged by the Flag epitope) together with pcDNA3.1(+)-3 $\times$ HA-Ub, before being treated with 10  $\mu$ mol/L of MG132. Then,  $\beta$ -catenin ubiquitination was assessed by *in vivo* ubiquitination assay (e). The total cell lysates were also subjected to Western blotting with either anti-Flag or anti-V5 antibodies (f). (g) A model is proposed to provide a better explanation of the mechanisms underlying  $\beta$ -catenin activation in Nrf1/TCF11-silenced cells. Two schematic diagrams show that the putative OFF- or ON-states of the Wnt/ $\beta$ -catenin signaling pathways are determined by the presence or absence of Nrf1, respectively. In fact, knockdown of Nrf1 resulted in obvious altered expression of most of the Wnt/ $\beta$ -catenin pathway components as illustrated diagrammatically.

degradation, particularly in the presence of MG132. Therefore, shNrf1- or shNC-expressing HepG2 cells had been cotreated with CHX (100  $\mu$ g/mL) and MG132 (5  $\mu$ mol/L) for the indicated lengths of time before Western blotting was conducted to determine whether  $\beta$ -catenin stability was influenced in Nrf1-silenced cells. As anticipated, the results revealed that silencing of Nrf1 caused a highly increased expression level of  $\beta$ -catenin (Figure 4(a)), and this protein stability was also retained with almost no or little effects on its half-life, as the chase time was extended from 0.5 to 8 h following treatment of shNrf1-expressing cells (Figure 4(b)). By contrast, treatment of shNC-expressing cells with proteasomal inhibitor MG132 initially stimulated a considerable higher expression abundance of  $\beta$ -catenin, but its protein stability was not maintained when the CHX chase time was increased (Figure 4(a)). The protein levels of  $\beta$ -catenin were then decreased to a lower level, with a short half-life of 2.96 h following cotreatment with CHX and MG132 (Figure 4(b)). In this chase course of shNC cells, the short-lived isoforms-A/B of Nrf1 also rap-

idly disappeared by 2 h, even after cotreatment with CHX and MG132, while smaller isoforms-C/D of Nrf1 was enhanced with a longer half-life of 7.82 h (Figures 4(a) and 4(b)). Together, these results presage that knockdown of Nrf1 leads to the stabilization of  $\beta$ -Catenin, albeit both protein stability was determined by the proteasomal degradation pathway.

Subcellular fractionation revealed that when compared to the shNC controls, silencing of Nrf1 caused an obvious increase in the total protein expression of  $\beta$ -catenin, which was recovered in the nuclear and cytosolic fractions but more abundantly localized in the nuclear, rather than the cytoplasmic, compartments (Figures 4 C1 and 4(d)). By sharp contrast, striking increases in the phosphorylated  $\beta$ -catenin at its Ser<sup>33</sup> and Ser<sup>37</sup> (both consensus sites of GSK-3 $\beta$  for targeting to TrCP-mediated ubiquitin proteasomal degradation) were observed in the cytoplasm of Nrf1-silenced cells (Figures 4(c), C2 and 4(c), C3 and 4(d)). Yet, this was accompanied by significant decreases of  $\beta$ -catenin phosphorylation in the nucleus of Nrf1-silenced cells. Furthermore, two longer



isoforms A/B of Nrf1 were recovered principally in the cytosolic fractions of shNC control cells, but almost not presented in the cytosolic and nuclear fractions of shNrf1-silenced cells (Figure 4(c), C4). Relatively, two close short isoforms C/D of Nrf1 (to become a mature factor) were recovered predominantly in the nucleus of shNC cells, but almost not observed in the nucleus of shNrf1-silenced cells. Collectively, these presage there exist distinct effects of Nrf1 on the cytoplasmic phosphorylation of  $\beta$ -catenin and its nuclear translocation.

Next, to examine the above putative effect of Nrf1 on potential ubiquitination of  $\beta$ -catenin, the human 293T cells were cotransfected with their two indicated expression constructs together with pcDNA3.1(+)-3 $\times$ HA-Ub and then treated with MG132. The *in vivo* ubiquitination of  $\beta$ -catenin immunoprecipitates (IP) with anti-Flag antibody was visualized by Western blotting with HA (UB) antibody (Figure 4(e)). The results unraveled that the immunoprecipitated  $\beta$ -catenin was ubiquitinated and also promoted only by overexpression of Nrf1 (Figures 4(e) and 4(f)).

Collectively, together with transcriptomic sequencing, a model was herein proposed (as illustrated in Figure 4(g)) to provide a better explanation of the underlying mechanism(s) by which either activation or inactivation of the  $\beta$ -catenin signaling towards target genes is dependent, respectively, on the absence or presence of Nrf1. Of note, most of all 26S proteasomal subunits are transcriptionally regulated by Nrf1, particularly in the proteasomal “bounce-back” response to its limited inhibitor [14, 24, 54]. When such function of Nrf1 was stably silenced, all three active subunits  $\beta$ 1,  $\beta$ 2, and  $\beta$ 5 (encoded by *PSMB6*, *PSMB7*, and *PSMB5*) of the 20S core proteasomal particle were downregulated in the shNrf1-expressing cells, which was roughly similar to those obtained from *Nrf1 $\alpha$ <sup>-/-</sup>* (HEA157) cells (Figure S5A, Table S2). Thus, it is inferable that albeit  $\beta$ -catenin was autophosphorylated by GSK-3 $\beta$ , it was not subjected to proteasomal degradation, thus, allowing for accumulation in the cytoplasm and nucleus of Nrf1-silenced cells (Figure 4(c), C1), such that differential expression of distinct target genes was regulated by Wnt/ $\beta$ -catenin signaling networks, as determined by transcriptomic sequencing (Figures 4(g), S5B).

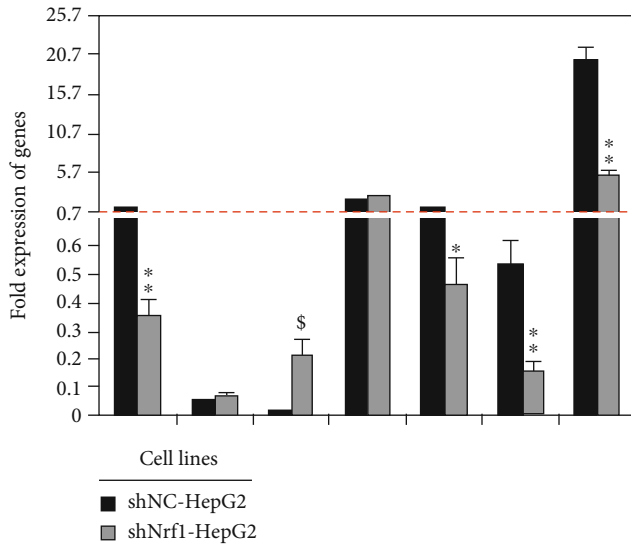
**3.7. Dysregulation of Wnt/ $\beta$ -Catenin Signaling and Relevant Response Genes in Nrf1-Silenced Tumor.** Transcriptomic analysis demonstrated that 34 of differential expression genes (DEGs) were obviously upregulated, while other 31 DEGs were downregulated or silenced by shNrf1 (Figure S5B). The upexpressed genes included *Wnt5A*, *Wnt11*, *PORCN*, *FZD10*, *CTNNB1*, *CTNNB1P1*, *APC2*, *CXXC5*, *LEF1*, *MMP7*, *TESC*, *CAMK2D*, *RAC3*, *LMCD1*, *CHP1*, *CCND1*, *PPP3CA*, *TMEM135*, *SKP1*, *JUN*, and *FOSL1*. Conversely, the downexpressed genes included *Wnt7A*, *FZD6*, *FZD8*, *DKK1*, *DIXDC1*, *LRP4*, *LRP6*, *DAAM1*, *CXXC4*, *TCF4* (i.e., *TCF7L2*), *GSK3B*, *FBXW11*, *RBX1*, *SEN2*, *NLK*, *PPP2R1B*, *PRKACA*, *PRKX*, *LRRF1P1*, *CTBP1*, *SMAD3*, *SMAD4*, *MYC*, and *TP53*. These collective data revealed that both Wnt/ $\beta$ -catenin-dependent and Wnt/ $\beta$ -catenin-independent signaling responsive genes were dysregulated in Nrf1-silenced cells (Figure 4(g) and Table S3). Of note, upregulation of *PORCN* by knockdown of Nrf1 is

postulated to trigger activation of the Wnt/ $\beta$ -catenin signaling networks, because all Wnts are lipid modified by porcupine, a specific palmitoyl transferase encoded by *PORCN*, in which this lipid moiety functions primarily as a binding motif for the Wnt receptors (e.g., FZD) and also renders all the Wnt proteins hydrophobically tethering to the cell membranes, thus, determining Wnt production, secretion, and range of action [51].

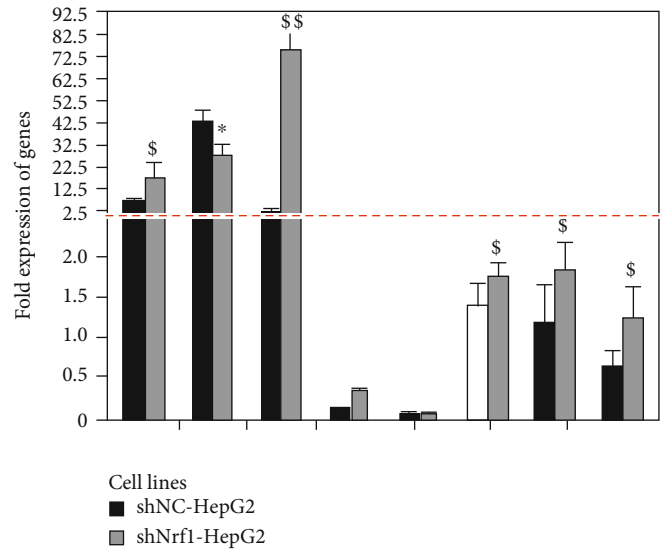
Here, further validation by real-time qPCR of Nrf1-silenced cells and xenograft tumors revealed that transcriptional expression of *CTNNB1* (encoding  $\beta$ -catenin) was almost unaffected by shNrf1 (Figures 5(a) and 5(c)), but a modest increase in *CTNNB1P1* (encoding  $\beta$ -catenin-interacting protein 1 to impede interaction of  $\beta$ -catenin with TCF factors) was observed (Figures 5(b) and 5(d)). Amongst the LEF/TCF family, expression of *LEF1* was upregulated, while *TCF4* is downregulated, upon silencing of Nrf1 (Figures 5(a)–5(d)). The latter notion is corroborated by immunohistochemical staining with TCF4 and Nrf1 antibodies (Figure 5(e)), indicating that TCF4 was obviously downexpressed in Nrf1-silenced tumor tissues, but not in the shNC controls. As such, it is not surprising that similar downregulation of TCF4, as a coactivator of  $\beta$ -catenin, was also observed in the human breast tumors as described by Shulewitz et al. [55]. Thereby, it is inferable that the LEF/TCF family proteins are functionally redundant in the Wnt/ $\beta$ -catenin signaling networks. This notion is based on the fact that, activation of the Wnt/ $\beta$ -catenin signaling occurs upon stable knockdown of Nrf1, even though TCF4 is downexpressed in such Nrf1-silenced cells.

Interestingly, three examined ligands *Wnt5A*, *Wnt11*, and *Wnt7A*, as well as its receptor *FZD10*, were enhanced by shNrf1 to different extents, but conversely no or few changes in mRNA expression of *AXIN1*, *APC2*, and *DVL1* (i.e., three intermediate components essential for Wnt/ $\beta$ -catenin signaling transduction) (Figures 5(a)–5(d)). Further examination of  $\beta$ -catenin/TCF-target genes demonstrated that transcriptional expression of *MMP10* was substantially augmented, but *SMAD4* and *MYC* were strikingly downregulated, upon knockdown of Nrf1 (Figures 5(a)–5(d)). Collectively, it is postulated that deficiency of Nrf1 leads to dysregulated transcription of some critical components of the Wnt/ $\beta$ -catenin signaling towards distinct target genes in the human hepatoma.

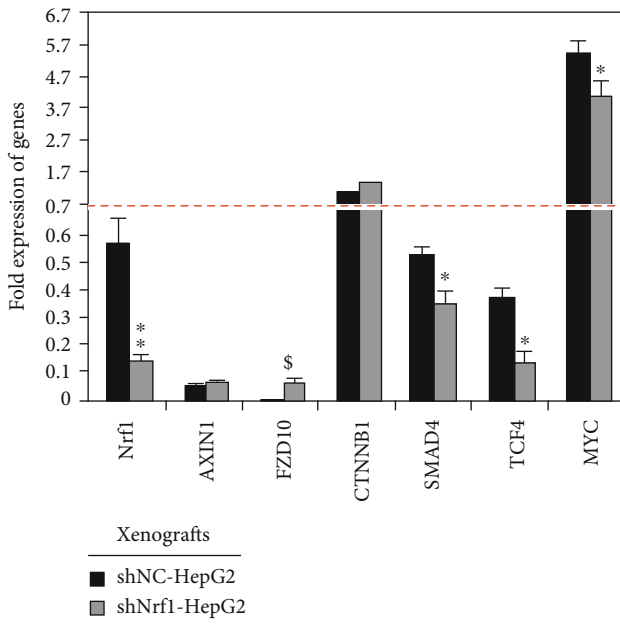
**3.8. Context-Dependent Expression of Wnt/ $\beta$ -Catenin Signaling Responsive Genes Is Relevant to Extents of Nrf1 Deficiency in Distinctly Differentiated Hepatoma.** Herein, real-time qPCR revealed that expression of *Nrf1* mRNA was almost completely abolished in distinct human hepatomas, by comparison with that of their corresponding *paracarcinoma* tissues (Figure S6A). This is also supported by Western blotting evidence that two major longer isoforms of Nrf1, particularly with a molecular mass of ~120 kDa, were also downexpressed in hepatoma tissues (Figure S6B, C). Furtherly, immunohistochemical staining manifested that protein expression of Nrf1 was substantially attenuated or almost abolished in distinct human hepatoma tissues, as coincident with pathological differentiation extents of



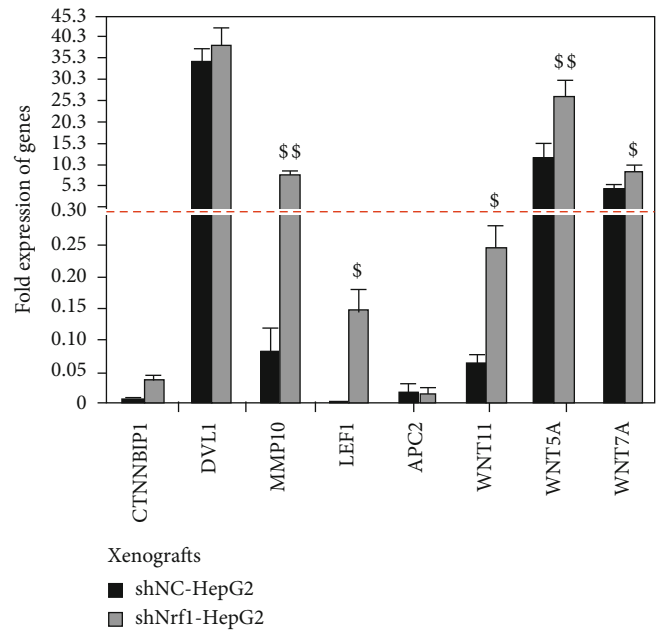
(a)



(b)



(c)



(d)

FIGURE 5: Continued.

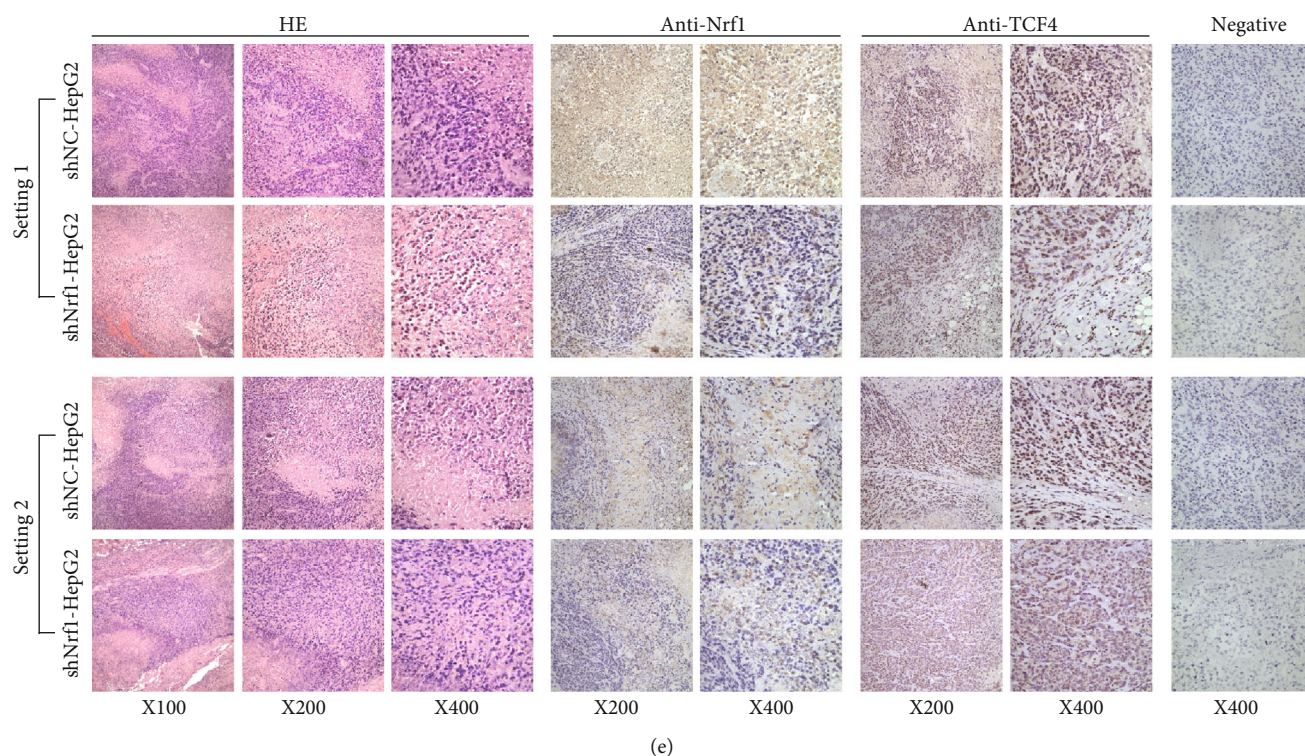


FIGURE 5: Dysregulation of the certain Wnt/ $\beta$ -catenin signaling response genes in Nrf1-silenced hepatoma cells. (a–d) Expression levels of *Nrf1* and those genes that are implicated in the putative Wnt/ $\beta$ -catenin signaling pathways in shNrf1- and shNC-expressing HepG2 cells (a, b), as well as in their derived subcutaneous xenograft tumors (c, d), were further determined by real-time qPCR. The data are shown as mean  $\pm$  SEM ( $n = 3 \times 3$ ), with significant increases ( $^{\text{S}}p < 0.05$ ;  $^{\text{SS}}p < 0.01$ ) and decreases ( $^*p < 0.05$ ;  $^{**}p < 0.01$ ) of shNrf1 compared to the shNC controls. (e) Two settings of subcutaneous xenograft tumor tissues were subjected to further evaluation by immunohistochemical staining with antibodies against Nrf1 or ATF4, in addition to the HE staining. The negative staining was set up by the nonimmune serum to replace the primary antibody in the parallel experiments. The resulting images were acquired in distinct microscopic fields.

cancer when compared to the corresponding *para*-carcinoma tissues (Figure S6D to F). This is supported by further evidence obtained from real-time qPCR (Figure S6G to I). Next, analysis of Wnt/ $\beta$ -catenin signaling components revealed that mRNA expression levels of *Wnt5A*, *CTNNB1P1*, *DVL1*, *SMAD4*, and *JUN* were detected in well-differentiated hepatoma but not in their *para*-carcinoma tissues (Figure S6G). Relatively, *FZD10* and *TCF4* were highly expressed in these *para*-carcinoma tissues but significantly reduced in the core carcinoma tissues. By contrast, most of the aforementioned genes *Wnt5A*, *CTNNB1P1*, *SMAD4*, *FZD10*, and *TCF4* were upexpressed predominantly in the *para*-carcinoma tissues of low poorly-differentiated hepatoma, with an exception of *DVL1* and *JUN* only emerged in the core hepatoma (Figure S6I). Intriguingly, *FZD10* and *LEF1* were only expressed in the medium-differentiated hepatoma but its *para*-cancer tissues, while a modest expression level of *DVL1* in this hepatoma was examined over that of the *para*-cancer tissues (Figure S6H). Such being the case, *Wnt5A*, *CTNNB1P1*, *SMAD4*, and *TCF4* was expressed primarily in the *para*-cancer tissues but were reduced to varying degrees in cancer tissues. In addition, a high expression level of *JUN* was indifferently retained in the medium-differentiated hepatoma and *para*-carcinoma tissues (Figure S6H). Taken altogether, these results imply that distinct extents of Nrf1 deficiency

might contribute to differential expression profiles of the Wnt/ $\beta$ -catenin signaling responsive genes, which could be involved context-dependently in the human liver cancer development and progression.

**3.9. Distinct Effects of Nrf1 on ARE-Luc Reporter Genes Constructed from Wnt/ $\beta$ -Catenin Signaling Components.** To gain an insight into distinct or even opposing effects of Nrf1 on the Wnt/ $\beta$ -catenin-dependent and Wnt/ $\beta$ -catenin-independent signaling, we here constructed several luciferase reporters from the representative gene promoters and their enhancer ARE/AP1-binding sequences (as listed in Table S4). As shown in Figure 6(a), ectopic expression of Nrf1 led to different extents of decreases in the four indicated reporter gene activity, driven by the longer promoters of *Wnt11*, *TCF4*, *LEF1*, or *JUN*. Similar results were also obtained from most of their respective enhancer ARE-driven luciferase assays (Figure 6(b)), with an exception that the *TCF4-ARE-luc* reporter activity was increased by ectopic Nrf1, but almost abolished by this ARE mutant. Furthermore, increased activity of the *JUN-ARE* mutant reporter was suppressed by Nrf1, but it had no effects on the *Wnt11-ARE4* mutant-led increase (Figure 6(b)).

Intriguingly, the *FZD10-promoter*-driven luciferase activity was almost unaffected by the Nrf1 expression (Figure 6(a)), but the *FZD10-ARE*-driven and its ARE mutant reporters were



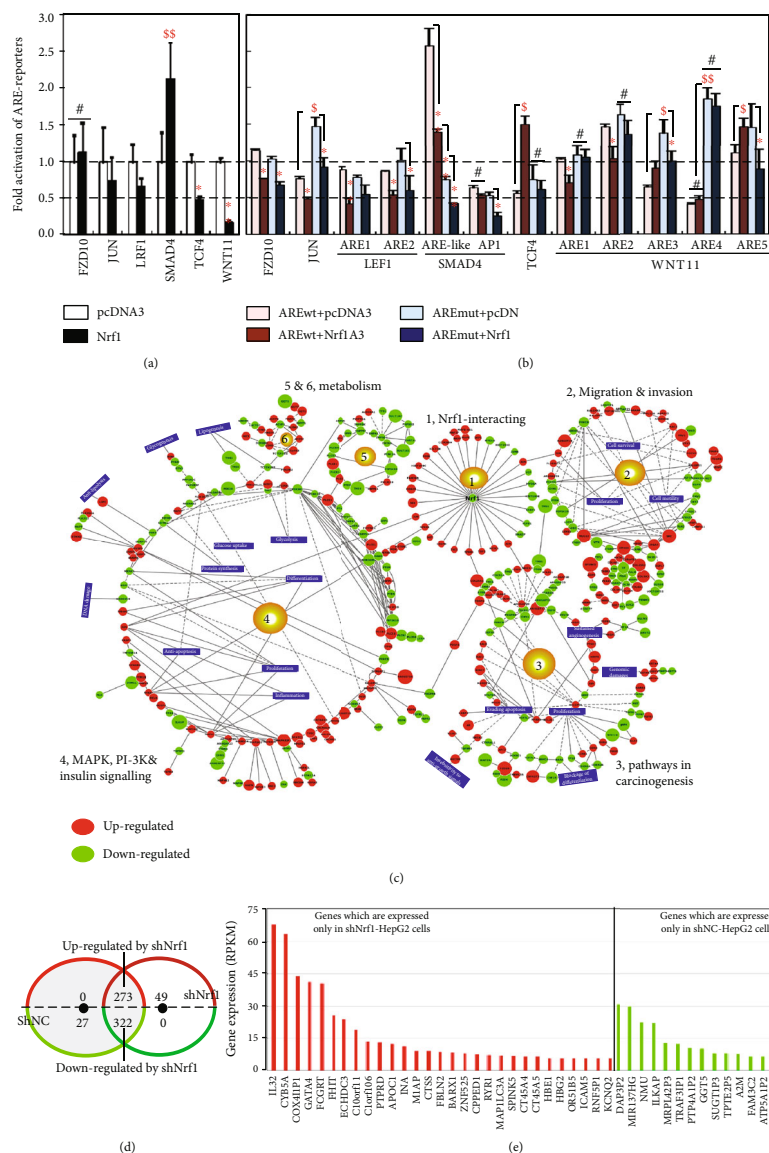


FIGURE 6: Oposing effects of Nrf1 on the Wnt/β-catenin signaling components, with its deficiency-leading alterations in the transcriptomic expression. (a) Distinct lengths of the gene promoters of *FZD10*, *JUN*, *LEF1*, *SMAD4*, *TCF4*, and *WNT11* (Table S4) were cloned into a luciferase reporter plasmid, respectively. Either of these indicated reporter genes, together with an internal control reporter pRL-TK and another expression construct for Nrf1 (or an empty pcDNA3 plasmid), were cotransfected into HepG2 cells and then allowed for a 24 h recovery before the luciferase activity was measured. The data are shown as mean ± SEM ( $n = 3 \times 3$ ), with a significant increase ( $^{\$}p < 0.05$ ) and significant decreases ( $^{*}p < 0.05$ ;  $^{**}p < 0.01$ ) being caused by ectopic Nrf1, relative to the pcDNA3 controls. No statistically significant differences are represented by #. (b) Several short lengths of AP1/ARE sequences were selected from the above genes (Table S4), along with pRL-TK and another expression construct for Nrf1 (or an empty pcDNA3 plasmid), were cotransfected into HepG2 cells and then allowed for a 24 h recovery before being measured. The luciferase activity data are shown as mean ± SEM ( $n = 3 \times 3$ ), with significant increases ( $^{\$}p < 0.05$ ;  $^{\$\$}p < 0.01$ ), significant decreases ( $^{*}p < 0.05$ ;  $^{**}p < 0.01$ ) or no statistic differences (#) being compared to the corresponding controls. (c) Schematic representation of an interactive network comprising Nrf1 interactors, and those key molecules that are implicated in cell migration and invasion, cancer development and progression, and signal transduction and metabolism pathways. Within the network, each road is built on the base of the corresponding pathways in the KEGG pathway database, while the nodes represent those genes involved in relevant pathways. Their colors and sizes vary with the fold changes of differential expression genes (DEGs) determined by transcriptomic sequencing of shNrf1 cells, by comparison to the equivalent shNC controls. Up- or downregulation of DEGs by shNrf1 was indicated in the red or green backgrounds, respectively. In addition, the node size reveals that the bigger the node, the larger the fold change. (d) A Venn diagram with distinct expression trends of DEGs, whose RPKM values are greater than 3 in at least one cell line (cf., shNrf1 with shNC cells). Amongst the DEGs, 27 genes were only expressed in shNC cells but completely silenced by shNrf1, whereas other 49 genes were only expressed in shNrf1 cells, and upregulated by knockdown of Nrf1. Further, 273 genes were upregulated by shNrf1, while other 322 genes were downregulated by shNrf1, albeit all these genes were coexpressed in two distinct cell lines. (e) Several representative genes that are only expressed in shNrf1 or shNC cells, each of which has an RPKM value of greater than 5.

modestly inhibited by this CNC-bZIP factor (Figure 6(b)). By contrast, a significant increase in the *SMAD4*-promoter-driven luciferase activity was mediated by Nrf1 (Figure 6(a)), albeit it also caused another remarkable decrease in the activity of the *SMAD4*-*API*/*ARE*-like enhancer (5'-TGAGTCAGG-3', with an AP1-binding site underlined), and further decrease was caused by its mutant (5'-TTCGGACGG-3' in Figure 6(b)). Also, the AP1-driven reporter gene activity was modestly inhibited by Nrf1. Collectively, these presage that distinct or opposite activity of Nrf1 to mediate differential transcription of ARE/AP1 battery genes may be dependent on different contexts of their enhancer-adjoining sequences encompassed within respective gene promoter regions.

**3.10. Significant Changes in the Wnt/ $\beta$ -Catenin-Independent Transcriptome of Nrf1-Silenced Cells.** The transcriptomic profiling of the genome-wide gene expression revealed that 20 of the top statistic significant pathways were herein enriched by comparison of shNrf1-silenced HepG2 cells with the shNC controls (Figure S7). Their multiple cross-talks between these pathways comprised a big complex regulatory network (Figure 6(c)). By perusing the detail information of DEGs (as deciphered in Table S5), those DEG-regulatory networks were much likely implicated in carcinogenesis, invasion, and metastasis. This was accompanied by shNrf1-directed reprogramming of cell metabolism, inflammatory and anti-inflammatory responses, and other processes (e.g., division, proliferation, and differentiation) (Figures 6(c) and S7).

By comparison with shNC-derived controls, 273 of DEGs were upregulated by silencing of Nrf1, while other 322 genes were downregulated (Figure 6(d)). Interestingly, 49 genes were expressed only in shNrf1-derived cells, but not in shNC control cells (Figure 6(d)). Relatively, 29 of higher expressed genes included *IL-32*, *CYB5A*, *COX4I1P1*, *GATA4*, *FCGRT*, *FHIT*, *ECHDC3*, *C10orf11* (i.e., *LRMDA*), *C10orf106* (i.e., *CDH23-AS1*), *PTPRD*, *APOC1*, *M1AP*, *INA*, *CTSS*, *FBLN2*, *BARX1*, *ZNF525*, *CPPED1*, *RYR1*, *SPINK5*, *MAP1LC3A*, *CT45A4*, *CT45A5*, *HBE1*, *HGB2*, *OR51B5*, *ICAM5*, *RNF5P1*, and *KCNQ2* (Figure 6(e), left panel and Table S6). Conversely, another 27 genes were almost completely silenced in shNrf1 cells, but they were expressed in shNC cells (Figure 6(d)), 16 of which included *DAP3P2*, *MIR137HG*, *NMU*, *ILKAP*, *MRPL42P3*, *TRAF3IP1*, *PTP4A1P2*, *GGT5*, *SUGTIP3*, *TPTE2P5*, *A2M*, *FAM3C2*, *ATP5A1P2*, *C3orf14*, *RCOR2*, and *SCGB3A2* (Figure 6(e), right panel and Table S6). Notably, further analysis by DAVID (the database for annotation, visualization, and integrated discovery) revealed that 8 of upregulated genes *APOC1*, *CPPED1*, *CYB5A*, *FBLN2*, *FHIT*, *PTPRD*, *RYR1*, and *SPINK5* could be involved in the functioning of extracellular exosome, but only 3 downregulated genes *A2M*, *NMU*, and *SCGB3A2* may also exert a certain effect on extracellular compartments, albeit whether such altered expression facilitates production and secretion of Wnt morphogens, and their receptors remain to be further determined. In addition, transcriptomic sequencing also unraveled that 31 of known genes critical for Nrf1-interacting proteins were also altered by shNrf1, when compared to shNC cells (Figure 6(c) and Table S5).

**3.11. Identification of Critical DEGs Involved in Nrf1-Deficient Hepatoma and Malignant Migration.** To scrutinize which DEGs are caused by Nrf1 deficiency resulting in cancer development, invasion, and metastasis, two heat maps were generated from the RNA-sequencing data. As shown in Figure 7(a), 45 of DEGs were identified to be responsible for shNrf1-led remodeling of cancer cell adhesion and extracellular matrix- (ECM-) receptor interaction, 22 of which were, however, completely abolished by knockout of *Nrf1 $\alpha$ <sup>-/-</sup>* (to yield a HepG2-derived HEA157 cell line, as described by our group [36]) (Table S7). Close comparison of related gene expression RPKM values revealed that 21 of DEGs involved in the cell adhesion and ECM-receptor interaction were upregulated by silencing of Nrf1, of which 7 genes (i.e., *MUC13*, *NRARP*, *RAC3*, *PDGFA*, *EGFL7*, *SDC3*, and *SRC*) were downregulated or completely blocked by *Nrf1 $\alpha$ <sup>-/-</sup>* (Figure S8A and Table S7). Amongst them, additional 6 genes (i.e., *AGRN*, *VAV2*, *EHBPI1L1*, *COL4A1*, *C19orf57*, and *MEGF8*) were almost unaffected by *Nrf1 $\alpha$ <sup>-/-</sup>*, when compared with wild-type controls. Further comparative analysis unraveled that silencing of Nrf1 led to obvious down-expression of 27 genes critical for cancer cell adhesion and ECM remodeling, of which 8 genes (i.e., *EGFR*, *CAV1*, *CAV2*, *MET*, *LRRF1P1*, *SDC1*, *TNS1*, and *CCDC77*) were almost unaltered by *Nrf1 $\alpha$ <sup>-/-</sup>*, but with an exception of 3 genes (*IGF1R*, *TPBG*, and *NEDD9*) that were strikingly upregulated by this knockout of *Nrf1 $\alpha$ <sup>-/-</sup>* (Figure S8A, and Table S7).

By construing another heat map (Figure 7(b)), 43 of DEGs were identified to be critical for the certain responsive pathways in shNrf1-derived hepatoma, 27 of which were almost not expressed in *Nrf1 $\alpha$ <sup>-/-</sup>*-derived HEA157 cells (see Table S8). Further insight into the cancer-related gene expression unraveled that 22 of DEGs were upregulated by shNrf1, of which 4 genes (i.e., *RAC3*, *PDGFA*, *GSTA4*, and *RXRA*) were downregulated by *Nrf1 $\alpha$ <sup>-/-</sup>* (Figure S8B, and Table S8). Conversely, 28 of cancer-related genes were downregulated by shNrf1, of which 6 genes (i.e., *HIF1A*, *STAT5B*, *IGF1R*, *TGFBR1*, *ATRN*, and *FZD6*) were upregulated by *Nrf1 $\alpha$ <sup>-/-</sup>* to varying extents. Rather, expression of additional 15 genes (i.e., *GSTP1*, *RALB*, *MECOM*, *FOXO1*, *CASP3*, *MEGF8*, *TMEM135*, *EGFR*, *MGST1*, *CTNNAL1*, *TNS1*, *FGFRL1*, *TCF4*, *CDKN2B*, and *CHN1*) was unaffected by *Nrf1 $\alpha$ <sup>-/-</sup>* in HEA157 cells, albeit they were significantly altered by shNrf1, when compared to those control values obtained from wild-type *Nrf1<sup>+/+</sup>* cells (Figure S8B, and Table S8). Taken together, it is inferable that Nrf1 deficiency results in constitutive activation and/or repression of putative Wnt/ $\beta$ -catenin-dependent and Wnt/ $\beta$ -catenin-independent signaling cascades in cancer development and malignant progression.

**3.12. Aberrant Activation of the PI3K-PDK1-AKT Signaling in Nrf1-Deficient Hepatoma Cells.** To corroborate the notion that deficiency of Nrf1 causes aberrant activation and/or repression of putative Wnt/ $\beta$ -catenin-independent signaling pathways, for example, the PTEN-PI3K-PDK1-AKT signaling cascades, were examined herein. Western blotting of protein separation by whole PAGE gels showed that expression of Nrf1 $\alpha$  and its derivatives, except for the minor Nrf1 $\beta$ , was

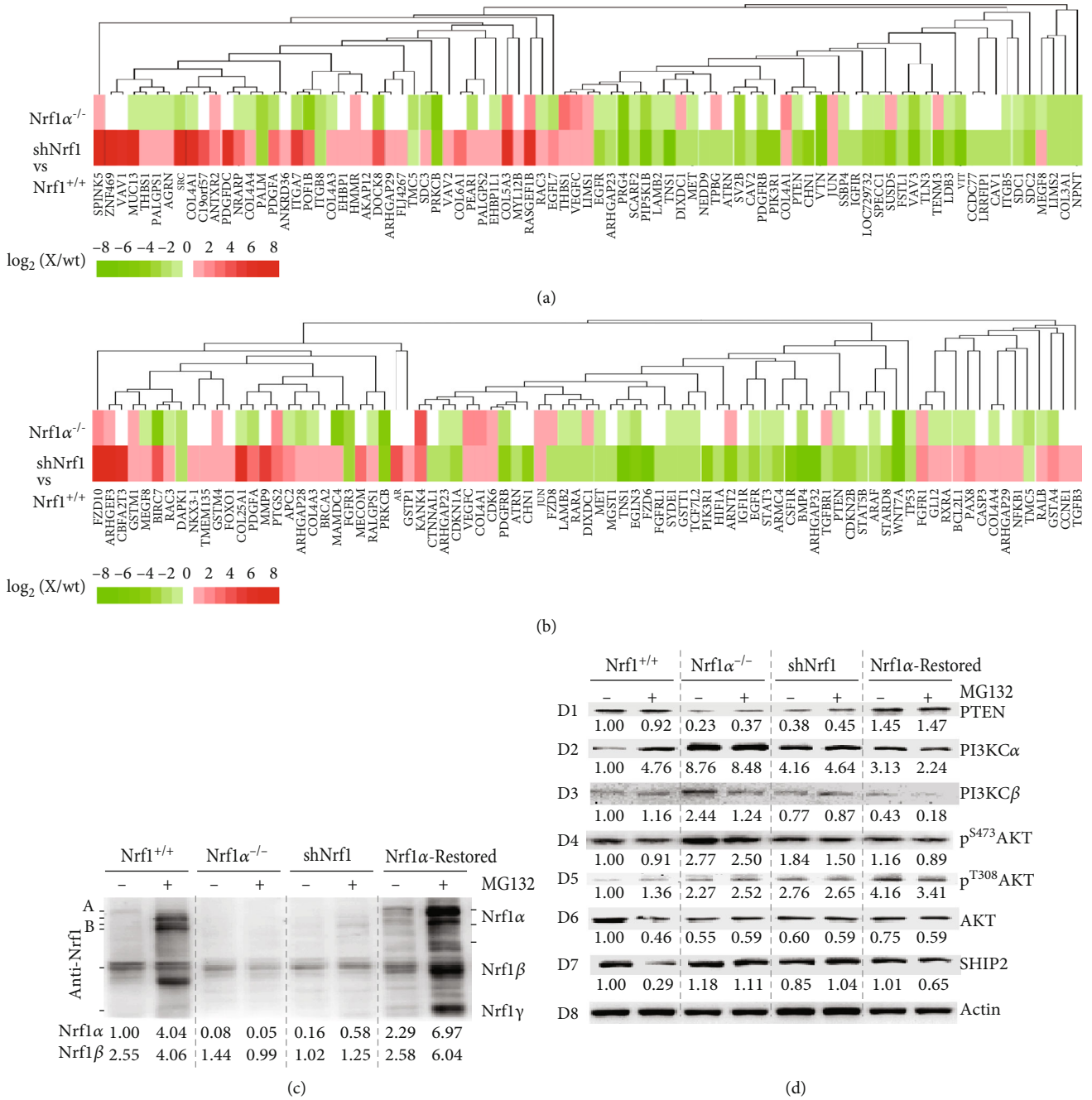


FIGURE 7: Continued.



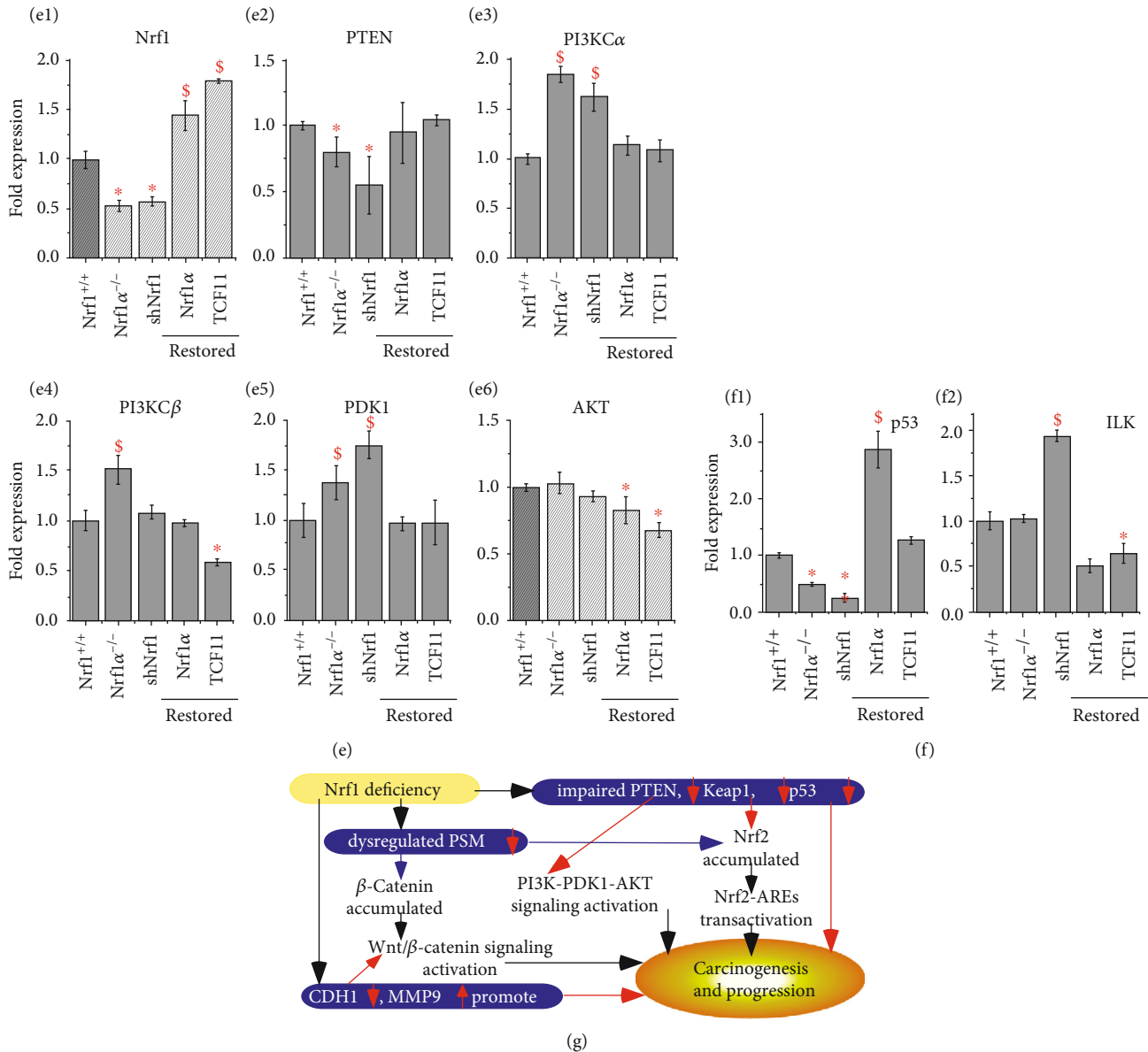


FIGURE 7: Activation of the PI3K-PDK1-AKT signaling and dysfunction of other pathways in Nrf1-deficient hepatoma. (a, b) Two heat maps of DEGs that are caused by Nrf1 deficiency resulting in putative invasion and metastasis (a) and cancer development (b). The heat maps were drawn with the sequencing expression of genes by the HemI software, then clustered by hierarchical clustering. The color of the nodes in the heat map is the value of  $\log_2$  (fold change) as shown in the color bars, indicating the gene expression trend compared with the control group (upregulation or downregulation were marked in red or green, respectively). Relevant results were also illustrated in supplemental Figure S8. (c) The abundances of distinct Nrf1 isoforms in *Nrf1*<sup>+/+</sup>, *Nrf1*<sup>-/-</sup>, shNrf1, and *Nrf1* $\alpha$ -restored cell lines were determined by Western blotting. The intensity of major immunoblots representing Nrf1 $\alpha$  and Nrf1 $\beta$  was quantified by the Quantity One 4.5.2 software and also shown on the bottom. (d) The above four cell lines (*Nrf1*<sup>+/+</sup>, *Nrf1*<sup>-/-</sup>, shNrf1, and *Nrf1* $\alpha$ -restored) had been treated with 5  $\mu$ mol/L of MG132 for 8 h before being visualized by Western blotting with the respective antibodies to detect the changes in these protein abundances of PTEN, PI3KC $\alpha$ , PI3KC $\beta$ , p<sup>S473</sup>AKT, p<sup>T308</sup>AKT, AKT, and SHIP2. The intensity of these blots was also quantified as shown on the bottom. (e, f) The mRNA expression levels of *Nrf1*, *PTEN*, *PI3KC $\alpha$* , *PI3KC $\beta$* , *AKT*, *PDK1*, *p53*, and *ILK* were determined by real-time qPCR analysis of *Nrf1*<sup>+/+</sup>, *Nrf1*<sup>-/-</sup>, shNrf1, *Nrf1* $\alpha$ -restored, and TCF11-restored cell lines. The data are shown as mean  $\pm$  SEM ( $n = 3 \times 3$ ). Significant decreases (\* $p < 0.05$ ; \*\* $p < 0.01$ ) and significant increases ( $^{\$}p < 0.05$ ) were statistically calculated as described above, when compared to wild-type *Nrf1*<sup>+/+</sup> controls. (g) A model is proposed to provide a clear explanation of aberrant activation of the Wnt/ $\beta$ -catenin signaling and the PI3K-PDK1-AKT pathway, as accompanied by dysfunction of other pathways, which are involved in Nrf1-deficient hepatoma development and progression.

abolished by loss of *Nrf1* $\alpha$ <sup>-/-</sup> HEA157 cells, but their minimum residues were retained in the MG132-stimulated shNrf1 cells (Figure 7(c)). Of note, all the indicated Nrf1 iso-

forms were restored in accordance with its mRNA expression in *Nrf1* $\alpha$ <sup>-/-</sup> cells that had been transfected with an expression construct for Nrf1 (or its long TCF11 form) (Figures 7(c) and

7(e), E1). Importantly, both protein and mRNA abundances of the tumor repressor PTEN were substantially suppressed by shNrf1 or *Nrf1* $\alpha^{-/-}$ , but this suppressive effect was completely recovered upon restoration of Nrf1 $\alpha$  or TCF11 into *Nrf1* $\alpha^{-/-}$  cells (Figures 7(d) D1 and 7(e) E2). Consequently, the basal protein and mRNA expression levels of PI3K $\alpha$  (phosphatidylinositol 3-kinase catalytic subunit  $\alpha$ , that serves as a direct target of PTEN) were augmented by shNrf1 or *Nrf1* $\alpha^{-/-}$  (Figures 7(d), D2 and 7(e) E3). Such active effects of Nrf1 deficiency on PI3K $\alpha$  were in a negative correlation with those of PTEN but are also strikingly repressed by Nrf1 $\alpha$  and TCF11 so as to be restored to the normal steady-state levels that were determined from wild-type *Nrf1* $^{+/+}$  control cells. Similarly, a modest increase in expression of PI3K $\beta$  was observed in *Nrf1* $\alpha^{-/-}$ , rather than shNrf1-expressing, cells, but also significantly inhibited by restored expression of Nrf1 $\alpha$  or TCF11 (Figures 7(d) D3 and 7(e) E4). Consistently, Western blotting of the murine subcutaneous carcinoma xenografts further prevented the evidence demonstrating that subverted inactivation of PTEN by *Nrf1* $\alpha^{-/-}$  was accompanied by constitutive activation of PI3K $\alpha$  and PI3K $\beta$  (Figure S9A). Further, insights into the *PTEN* promoter region unveiled that transcriptional expression of this gene was controlled by its ARE enhancers (Figure S9B, C).

Further examinations revealed that the mRNA expression of PDK1 (3-phosphoinositide-dependent protein kinase 1) was elevated by shNrf1 or *Nrf1* $\alpha^{-/-}$  and this elevation was turned down by Nrf1 $\alpha$  or TCF11 for a recovery to the wild-type level (Figure 7(e), E5). By contrast, the basal mRNA expression of AKT appeared to be unaffected by a deficiency of Nrf1, but modestly reduced by forced expression of Nrf1 $\alpha$  or TCF11 in *Nrf1* $\alpha^{-/-}$  cells (Figure 7(e), E6). Accordingly, the total protein abundance of AKT was roughly unaltered by shNrf1 or *Nrf1* $\alpha^{-/-}$  (Figure 7(d), D6). However, distinct increases in the major Ser<sup>473</sup>- and minor Thr<sup>308</sup>-phosphorylated proteins of AKT were determined in *Nrf1* $\alpha^{-/-}$  or shNrf1 cells (Figures 7(d), D4 and 7(d), D5). Conversely, restoration of Nrf1 $\alpha$  also enabled constitutive autophosphorylation of AKT at Ser<sup>473</sup>, but not at Thr<sup>308</sup> to be attenuated indeed. Further determination of the mouse subcutaneous carcinoma xenografts unraveled that total and phosphorylated proteins of AKT were markedly augmented in *Nrf1* $\alpha^{-/-}$ -derived tumor tissues (Figure S9A). Besides, an intriguing increase in expression of SHIP1 (Src homology 2-containing inositol-5'-phosphatase 1, that can enable inactivation of the PI3K-AKT signaling pathway) was observed in *Nrf1* $\alpha^{-/-}$ -derived tumor, albeit it was almost unaltered in the initially-inoculated *Nrf1* $\alpha^{-/-}$  cells, when compared with the wild-type controls (Figures 7(d) D7 and S9A).

It is a big surprise that the expression of the tumor repressor p53 was substantially blocked or abolished by shNrf1 or *Nrf1* $\alpha^{-/-}$  (Figure 7(f) F1). Conversely, restoration of TCF11 enabled for recovery of p53 from its disruptive expression by *Nrf1* $\alpha^{-/-}$ . Of note, inactivation of p53 by *Nrf1* $\alpha^{-/-}$  was not only reversed by Nrf1 $\alpha$  but also upregulated by this CNC-

bZIP factor to a considerable higher level, when compared with the wild-type *Nrf1* $^{+/+}$  control (Figure 7(f) F1). By contrast, the transcriptional expression of *ILK* (integrin-linked kinase) was significantly augmented by shNrf1, but not by *Nrf1* $\alpha^{-/-}$ , albeit most of its basal and increased abundances were markedly repressed by Nrf1 $\alpha$  or TCF11 (Figure 7(f) F2). In addition, the transcriptional activity of five luciferase reporter genes was driven by ARE-batteries existing in the promoter regions of *p53*, *CDH1*, *MMP9*, *VAV1*, and *PDGFB*, but also inactivated by their ARE mutants (Figure S9B and Table S9). Altogether, these results have demonstrated that loss of Nrf1 leads to constitutive inactivation of PTEN and p53, as accompanied by activation of the PI3K-PDK1-AKT signaling and other cascades, besides the putative activation of Wnt/ $\beta$ -catenin signaling (as proposed for a model in Figure 7(g)).

#### 4. Discussion

In the present study, we have corroborated the axiomatic rationale that Nrf1 is endowed with a dominant tumor-preventing function against human liver cancer development and malignant progression. Such tumor-repressing effect of Nrf1 is aroused by its intrinsic inhibition of Wnt/ $\beta$ -catenin signaling and independent cascades (e.g., AP-1), whilst concurrent activation of other tumor repressors, such as PTEN and p53, is also triggered by this CNC-bZIP factor.

**4.1. Function of Nrf1 Is Exerted as a Dominant Tumor Repressor in Defending Liver Carcinogenesis and Malignancy.** An earlier study revealed that gene-targeting knockout of all Nrf1 isoforms (i.e., *Lcrf1*<sup>tm1uab</sup>) in the mouse leads to a failure to form the primitive streak and mesoderm, dying at E6.5–E7.5 [25], implying it is essential for gastrulation in the early embryonic development. The defect of *Nrf1* $^{-/-}$  was also construed in a non-cell-autonomous way because the deficient embryonic stem cells (ESCs) were rescued in the chimeric mice during *in vitro* differentiation. Another non-cell-autonomous defect in global *Nrf1* $^{-/-}$  embryos (created by knocking-in to yield *Nrf1*<sup>rPGK-neo</sup> such that its DNA-binding domain-encoding sequence was disrupted in most of the distinct Nrf1 isoforms) leads to the lethality at mid-late gestation (i.e., E13.5–E16.5) from severe anemia, which results from abnormal maturation of precursor cells in fetal liver microenvironment [26]. Yet, no contribution of the *Nrf1* $^{-/-}$  ESCs to adult hepatocytes was traced during organ development of chimeric mice [56]. This defect was initially thought to be the consequence of oxidative stress [27, 56]; such oxidative stress is reinforced by double knockout of *Nrf1* $^{-/-}$ :*Nrf2* $^{-/-}$  [31]. Notably, a later study unveiled that the proteasomal “bounce-back” response to a low concentration of its inhibitor MG132 was substantially abolished by *Nrf1* $^{-/-}$ , but not *Nrf2* $^{-/-}$  [57], albeit murine Nrf1-deficient cells retained minimum abundances of residual proteoforms. Such compensatory proteasomal response mediated by Nrf1 has been further validated by the supportive evidence obtained from knockdown of human Nrf1 by siRNA or shRNA [54, 58] and knockout of human *Nrf1* $\alpha$  [14], as well

as its stable expression system [46]. Collectively, these demonstrate that *de novo* synthesis of compensatory proteasomes is determined by Nrf1, but conversely, its deficiency leads to an impaired expression profile of proteasomal subunits and thereby caused an aberrant accumulation of Nrf2 [23] and  $\beta$ -catenin (referenced in this study, Figure 7(g)).

As a matter of fact, Nrf1 is essential for the mature of fetal hepatocytes contributing to the adult liver because of widespread apoptosis of *Nrf1*<sup>-/-</sup>-derived hepatocytes during the late development of chimeric embryos [56]. Further, liver-specific knockout of *Nrf1*<sup>-/-</sup> in adult mice results in the spontaneous development of nonalcoholic steatohepatitis and hepatoma [28]. Significantly, the precancerous lesions are interrelated with hepatic steatosis, apoptosis, necrosis, inflammation, and fibrosis that was manifested in *Nrf1*<sup>-/-</sup> livers. Such typical pathology was investigated to result from severe oxidative stress and relevant damages, as a consequence of dysregulation of some ARE-battery genes by *Nrf1*<sup>-/-</sup> [28]. Besides, impaired transcription of proteasomes caused accumulation of ubiquitinated and oxidative damaged proteins in *Nrf1*<sup>-/-</sup> hepatocytes with steatosis [59]. Further determination also unraveled that, except Nrf1-dependent genes (e.g., *Mt1/2*, *Clrf*, *Gcn20*, *Gadd45 $\gamma$* , *Mfsd3*, and *Pdk4*), another subset of ARE-driven genes were transactivated predominantly by Nrf2 in adaptive response to endogenous oxidative stress arising from knockout of *Nrf1*<sup>-/-</sup>, because their transactivation was terminated by double knockout of *Nrf1*<sup>-/-</sup>:*Nrf2*<sup>-/-</sup> [29]. Overall, these facts demonstrate that Nrf1 is required for the basal constitutive expression of cytoprotective genes against cellular stress that activates Nrf2. Contrarily, loss of Nrf1 could also contribute, in a cell-autonomous way, to tumorigenesis caused by the chromosome mis-segregation [60]. Together, it is inferable that Nrf1 is endowed with its intrinsic function as a tumor suppressor in defending liver cancer development. This notion is further corroborated by our experimental evidence obtained from silencing of human Nrf1 (in this study), as well as knockout of human *Nrf1 $\alpha$*  [23, 36].

Herein, we have presented the evidence showing that silencing of Nrf1 by stable shRNA interference significantly promotes malgrowth of the human hepatocellular carcinoma, particularly its subcutaneous tumorigenesis accelerated in the xenograft model mice. Such knockdown of Nrf1 also enhances malignant invasion of the hepatoma and distant metastasis into the liver and lung of nude mice. Similar results were also obtained from knockout of human *Nrf1 $\alpha$*  [23, 36]. In the parallel xenograft experiments, the *shNrf1*-driven tumor appears to be a little more severe than the case of *Nrf1 $\alpha$* <sup>-/-</sup> (with aberrant accumulation of Nrf2), by comparison of subcutaneous tumorigenesis in speeds and sizes, as accompanied by cancer metastasis and cachexia syndromes (compare this work with our previous [36]). However, such severe conditions of *Nrf1 $\alpha$* <sup>-/-</sup>-driven tumors are significantly mitigated by additional silencing of Nrf2 (to yield *Nrf1 $\alpha$* <sup>-/-</sup>+*siNrf2*) [23]. By contrast, wild-type *Nrf1/2*<sup>+/+</sup>-bearing tumors are also strikingly ameliorated by *Nrf2*<sup>-/- $\Delta$ TA</sup> (with genomic deletion of transactivation domains of Nrf2), but roughly unaffected by *caNrf2*<sup>-/ $\Delta$ N</sup> (serves as a constitutive activator due to a loss of the N-

terminal Keap1-binding domain of Nrf2) [23]. Collectively, these facts authenticate that Nrf2 acts as a tumor promoter, whereas Nrf1 functions as a dominant tumor repressor and also confines oncogenicity of Nrf2. In turn, transcriptional expression of Nrf1 is positively regulated by Nrf2 through the former promoter [23]; the latter CNC-bZIP factor is marginally reduced in *shNrf1*-derived cells (Figure S9D), along with decreased expression of ARE-driven genes, e.g., *NQO1*. Such these differences between *shNrf1*- and *Nrf1 $\alpha$* -driven tumors are much likely to be determined by distinct decreased extents of multiple Nrf1 isoforms and its effects on Nrf2 and ARE-driven genes. In addition, it should be noted that substantial down-expression of Nrf1 in the clinic human hepatoma tissues is closely relevant to distinct cancer differentiations (Figure S6 and [36]), albeit the underlying mechanism(s) remains elusive.

**4.2. Activation of Wnt- $\beta$ -Catenin Signaling Implicated in Nrf1-Deficient Hepatoma Development and Progression.** Insights into the pathobiological mechanisms of Nrf1-deficient hepatoma have discovered that ubiquitin-mediated proteasomal degradation of  $\beta$ -catenin is seriously impaired by silencing of Nrf1 so that it is accumulated and translocated into the nucleus, leading to Wnt/ $\beta$ -catenin-mediated transcriptional activation of target genes. Notably,  $\beta$ -catenin is a key core component of the Wnt signaling cascades; this canonical pathway has been also accepted as a highly conserved and tightly controlled molecular mechanism that regulates important physiological and pathological processes in development, health, and disease (e.g., cancer) of multicellular organisms from early metazoan to human [51, 52]. Global knockout of  *$\beta$ -cat*<sup>-/-</sup> in mice leads to embryonic death at ~E7.0 from no formation of a primitive streak for mesoderm [61]; this is well coincident with the consequence of *Lcrf1*<sup>tm1uab</sup> [25]. Similar observations of *Wnt3*<sup>-/-</sup>, *Lrp5*<sup>-/-</sup>, *Lrp6*<sup>-/-</sup>, or  *$\beta$ -cat*<sup>-/-</sup> mice were obtained [62–64]. These construe that these components of the Wnt/ $\beta$ -catenin signaling pathway, along with Nrf1, are essential for gastrula development. Further, hepatocyte-specific conditional knockout of  *$\beta$ -cat*<sup>-/-</sup> or other genes indicates that the Wnt/ $\beta$ -catenin pathway is critical for the formation of adult liver from the early embryonic stages and its homeostatic maintenance by dictating relevant cell fates and polarity during development and growth [38, 39]. Rather, in adult tissues, the signaling pathway remains inactive within differentiated cells (at an OFF-state), although it regulates liver regeneration by controlling hepatocyte division, proliferation, as well as cell adhesion. This is owing to the considerable low expression of  $\beta$ -catenin because it is subjected to proteasomal degradation (Figures 4 and S10). The  $\beta$ -catenin destruction is incremented by induced proteasomal “bounce-back” response to its limited inhibitors but almost abolished by silencing of Nrf1 as a direct transactivator of proteasomes. Besides, downregulation of E-cadherins (encoded by *CDH1*), along with ILK, by knockdown of Nrf1 also causes  $\beta$ -catenin to be rapidly released from the plasma membrane-tethered adhesion complex and translocated into the nucleus. Thereby, the total nonphosphorylated

protein of  $\beta$ -catenin is accumulated in the nucleus, resulting in aberrant expression profiles of  $\beta$ -catenin-associated transcription factor (e.g., LEF/TCF, HIF1 $\alpha$ , FOXO, and SOX) target genes. Accordingly, an increase in the  $\beta$ -catenin/TCF-mediated TOP/FOP reporter gene activity is caused by silencing of Nrf1 (i.e., at an ON-state).

As discovered by our data, the Wnt/ $\beta$ -catenin signaling is constitutively activated by knockdown of Nrf1. However, such deficiency of Nrf1 led to downregulation of TCF4 (as a critical transcription partner of the  $\beta$ -catenin coactivator) in human Nrf1-silenced hepatoma xenografts and metastatic tumor tissues. Such seemingly confusing result appears to be coincident with the previously “surprising” finding by Shulewitz et al. [55]. Thereby, it is postulated that though TCF4 was *bona fide* down-expressed in Nrf1-silenced cells, the LEF/TCF family factors are also functionally redundant in the human Wnt/ $\beta$ -catenin signaling activation stimulated by deficiency of Nrf1, as identified by Hrckulak et al. [65] that TCF4 is dispensable for the Wnt signaling in human cancer cells. Notably, there exist 671 DEGs identified by transcriptomic sequencing in Nrf1-silenced cells (Table S6), of which  $\sim 77$  genes are implicated in the Wnt/ $\beta$ -catenin signaling and relevant responsive effects on target gene transcription, cell division cycle, cell proliferation, and differential fates, as well as cell polarity, cell adhesion, and cytoskeleton (Table S3). Altered or opposed expression of this complex signaling cascades and responsive genes are postulated to be context-dependent. This is determined plausibly by the tempo-spatial positioning of putative *cis*-regulatory elements (e.g., *ARE* and *API*- and *TCF*-binding sites) within distinct gene promoters, enabling recruitment of distinct transcription factor complexes with cognate partners existing in different differentiated cancer cells. In addition, it cannot be ruled out that potential positive and negative feedback loops are encompassed within this pivotal signaling-to-gene regulatory network.

Significantly, the Wnt/ $\beta$ -catenin signaling can polarize cells at their contact sites, orienting the axis of cell division while simultaneously programming daughter cells to adopt diverging differential fates in a tempo-spatially stereotyped way [52]. The coupling of cell fate to position enables for construction of the planning body by generating cellular diversity and spatial forms. Such a coupling system for the body plan of organized tissues and organs is likely broken in Nrf1-deficient cells within severe endogenous oxidative microenvironments. In the case, the directed differentiation of a variety of multipotent progenitor stem cells in the developing embryos and in the adult regenerating liver cannot be maintained in a robust homeostatic state. Consequently, a portion of these stem cells are disordered and derailed from the organized body plan insomuch as to generate a highly tumorigenic subpopulation of cancer cells, which are called tumor-initiating cells (as described by Nguyen et al. [66]). Thereby, we speculate that activation of the Wnt/ $\beta$ -catenin signaling network (and/or altered expression of its dominant components) is implicated in Nrf1-deficient hepatoma development and malignant progression.

In effect, the signaling by a family of the secreted Wnt morphogens governs developmental, homeostatic, and path-

ological processes by regulating  $\beta$ -catenin stability and its cooperative transcription factors to control downstream gene expression. Thus, Wnt/ $\beta$ -catenin signaling could represent a critical target for cancer, particularly while certain mutagenesis had been acquired in a host of cancer development. Of note, the solid evidence that has been provided in the present study and our previous work [23, 36] demonstrate that Nrf1 deficiency causes constitutive activation of the Wnt/ $\beta$ -catenin signaling, as accompanied by transcriptional induction of EMT, and relevant morphological changes in cell shape. Such EMT also promotes cancer cell migration, invasion, and distant metastasis, e.g., to the liver and lung, particularly when cell adhesion junction with the ECM-receptor interaction networks had been remodeled by activated MMP and inactivated cadherins (in cooperation with other altered molecules, as listed in Table S7).

**4.3. Involvement of Wnt/ $\beta$ -Catenin-Independent Networks in Nrf1-Deficient Carcinogenesis and Progression.** Collectively, the conserved Wnt/ $\beta$ -catenin signaling is construed as a living fossil for the specification of patterned multicellular animals by coupling distinct cell fate cascades with the proper spatial forms polarized along the primary anterior-posterior axis [52]. The topobiologically-organized body plan has been established by integral cooperation of the Wnt/ $\beta$ -catenin signaling with the BMP- and TGF $\beta$ -SMAD pathways, that are, respectively, exploited to create the dorsal-ventral and left-right axes running perpendicularly to the primary body axis. Thus, it is inferable that aberrant expression of the BMP- and TGF $\beta$ -SMAD signaling molecules, besides the Wnt/ $\beta$ -catenin cascades, contributes to cell-shape changes in Nrf1-deficient EMT process. Such altered polarity of Nrf1-silenced cell shape, as well as its oncogenic proliferation and migration, may be attributed to  $\beta$ -catenin-independent activation of the JNK-JUN signaling and API-target genes (in this study and [23]). Our evidence also demonstrates that deficiency of Nrf1 causes inactivation of two tumor repressors PTEN and p53, concurrently with oncogenic activation of the PI3K-PDK1-AKT signaling (Figure 7(g)). In addition, the MAPK signaling activation and aberrant cell metabolisms are also identified by transcriptomic sequencing to have been involved in Nrf1-deficient liver cancer development and malignancy (Tables S5, S8).

## 5. Conclusions

In summary, our evidence corroborates that Nrf1 functions as a dominant tumor repressor by intrinsic inhibition of the Wnt/ $\beta$ -catenin pathways and other signaling networks involved in human hepatoma development and progression. Herein, aberrant activation of this Wnt/ $\beta$ -catenin signaling by impairment of the core proteasomal subunits is much likely to play a pivotal role in orchestrating Nrf1-deficient liver carcinogenesis, progression and malignancy. As such, the pathological event occurs in particular dependence on severe endogenous oxidative stress and potential damages resulting from Nrf1-deficient cells, albeit hyperactivation of antioxidant factor Nrf2 (but with no alternations of its and



other homologous mRNA levels, Figure S9D). The further transcriptomic analysis provides a panoramic view of the Wnt/ $\beta$ -catenin-dependent and -independent signaling networks, together with related responsive gene expression profiling of the Nrf1-deficient hepatoma. Of note, dysregulated expression of putative Nrf1-target genes (e.g., *PTEN*, *CHD1*, *p53*, *MMP9*, *SMAD4*, *TCF4*, and *Wnt11*) is implicated in Nrf1-deficient liver cancer development and malignant behavior, albeit the detailed mechanisms are required to be further determined in the future. Overall, unraveling the unique function of Nrf1, which is distinctive from Nrf2, in liver cancer malignancies is likely to lead to novel preventive and therapeutic strategies to be paved against human cancer.

## Abbreviations

AP1:	Activator protein 1
ARE:	Antioxidant response element
bZIP:	Basic-region leucine zipper
CDH1:	Cadherin 1
CHX:	Cycloheximide
CNC:	cap'n'collar
CTNBN1:	Catenin $\beta$ 1
DEGs:	Differentially expressed genes
ECM:	Extracellular matrix
LEF1:	Lymphoid enhancer binding factor 1
luc:	Luciferase
EMT:	Epithelial-mesenchymal transition
Nrf1:	Nuclear factor-erythroid 2-related factor 1
TCF4:	T-cell-specific transcription factor 4 (also called TCF7L2).

## Data Availability

All data needed to evaluate the conclusions in the paper are present in this publication along with the 'Supplementary Information' that can be found online. Additional other data related to this paper may also be requested from the senior authors (with a lead contact at the Email: yiguo Zhang@cqu.edu.cn, or eaglezhang64@gmail.com).

## Disclosure

Besides, it should also be noted that the preprinted version of this paper had been initially posted at the bioRxiv 726349.

## Conflicts of Interest

The authors declare no conflict of interest.

## Authors' Contributions

J.C., M.W., X.R., Y.X., and Y.R. performed all most of the experimental work with bioinformatic analysis, collected their original data, and made a draft of all figures. Of note, M.W. also carried out most of the transcriptomic analysis and edited this manuscript with most of the figures and supplementary data. X.L. and L.Q. helped them to have done some biochemical and animal experiments. Lastly,

Y.Z. designed this study, analyzed all the data, helped to prepare all figures, and wrote and revised the paper. Jiayu Chen, Meng Wang, and Yuancai Xiang contributed equally to this work.

## Acknowledgments

We are greatly thankful to Professor Libo Yao (at State Key Laboratory of Cancer Biology, Department of Biochemistry and Molecular Biology, Air Force (Fourth Military) Medical University, No. 169 Changle-Xi Road, Xincheng District, Xi'an 710032, Shaanxi, China) for having provided part of workable space with initial supervision of Dr. Jiayu Chen. We also thank Mr. Zhengwen Zhang (Glasgow Dental Hospital and School, University of Glasgow and National Health Service, Scotland, UK) for his kind help in correcting the English language throughout this manuscript. The study was supported by the National Natural Science Foundation of China (NSFC, with two key programs 91129703, 91429305, and a project 81872336) awarded to Prof. Yiguo Zhang (Chongqing University, China). This work is also, in part, funded by Sichuan Department of Science and Technology grant (2019YJ0482) to Dr. Yuancai Xiang (Southwest Medical University, Sichuan, China).

## Supplementary Materials

*Supplementary 1.* Figure S1: expression of Nrf1/TCF11 and NQO1 in three pairs of shNrf1- and shNC-expressing cell lines that were treated with 10  $\mu$ mol/L of MG132 or vehicle control (DMSO) for 4 h. Figure S2: distinct expression levels of multiple Nrf1 isoforms. Figure S3: significant increments in the migration and invasion of Nrf1-silenced hepatoma cells. Figure S4: obvious changes in shNrf1-expressing cell viability, colony formation, cell cycle, and its apoptotic rate. Figure S5: comparison of differential expression genes in distinct genotypic cell lines. Figure S6: context-dependent expression of Wnt/ $\beta$ -catenin signaling responsive genes on distinct extents of Nrf1 deficiency in human hepatomas with different differentiation. Figure S7: scatter plot of the enriched KEGG pathways. Figure S8: significant differences in the expression of genes involved in cancer related pathway, focal adhesion, and ECM-receptor interaction. Figure S9: aberrant activation of the PI3K-PDK1-AKT signaling in Nrf1-deficient hepatoma cells.

*Supplementary 2.* Table S1: the key resources used in this work. Table S2: the sequencing data of genes encoding proteasomal subunits. Table S3: the sequencing data of genes involved in Wnt/ $\beta$ -catenin signaling pathway. Table S4: the promoters, the enhancer ARE/AP1-binding sequences, and the corresponding mutation sequences of the representative genes of Wnt/ $\beta$ -catenin signaling components. Table S5: the sequencing data of genes involved in the interactive network of Nrf1 interactors, migration and invasion pathways, carcinoma related pathways, signal transduction pathways, and metabolism pathways. Table S6: the sequencing data of DEGs whose RPKM values are greater than 3 in at least one cell line (shNC- or shNrf1-HepG2). Table S7: the sequencing data of genes implicated in the focal adhesion and ECM-

receptor interaction. Table S8: the sequencing data of genes responsible for the pathways involved in cancer. Table S9: the promoters, the enhancer ARE-binding sequences, and the corresponding mutation sequences of PTEN, p53, CDH1, VAV1, PDGFB, and MMP9.

## References

- [1] I. Slesak, M. Kula, H. Slesak, Z. Miszalski, and K. Strzalka, "How to define obligatory anaerobiosis? An evolutionary view on the antioxidant response system and the early stages of the evolution of life on earth," *Free Radical Biology and Medicine*, vol. 140, pp. 61–73, 2019.
- [2] H. Sies, C. Berndt, and D. P. Jones, "Oxidative stress," *Annual Review of Biochemistry*, vol. 86, no. 1, pp. 715–748, 2017.
- [3] L. B. Doonan, A. Hartigan, B. Okamura, and P. F. Long, "Stress-free evolution: the Nrf-coordinated oxidative stress response in early diverging metazoans," *Integrative and Comparative Biology*, vol. 59, no. 4, pp. 799–810, 2019.
- [4] Y. P. Zhu, M. Wang, Y. Xiang et al., "Nach is a novel subgroup at an early evolutionary stage of the CNC-bZIP subfamily transcription factors from the marine bacteria to humans," *International Journal of Molecular Sciences*, vol. 19, no. 10, article 2927, 2018.
- [5] K. Mukaigasa, L. T. Nguyen, L. Li, H. Nakajima, M. Yamamoto, and M. Kobayashi, "Genetic evidence of an evolutionarily conserved role for Nrf2 in the protection against oxidative stress," *Molecular and Cellular Biology*, vol. 32, no. 21, pp. 4455–4461, 2012.
- [6] Y. Zhang and Y. Xiang, "Molecular and cellular basis for the unique functioning of Nrf1, an indispensable transcription factor for maintaining cell homeostasis and organ integrity," *Biochemical Journal*, vol. 473, no. 8, pp. 961–1000, 2016.
- [7] G. P. Sykiotis and D. Bohmann, "Stress-activated cap'n'collar transcription factors in aging and human disease," *Science Signaling*, vol. 3, no. 112, article re3, 2010.
- [8] M. Yamamoto, T. W. Kensler, and H. Motohashi, "The KEAP1-NRF2 system: a thiol-based sensor-effector apparatus for maintaining redox homeostasis," *Physiological Reviews*, vol. 98, no. 3, pp. 1169–1203, 2018.
- [9] Y. Zhang, D. H. Crouch, M. Yamamoto, and J. D. Hayes, "Negative regulation of the Nrf1 transcription factor by its N-terminal domain is independent of Keap1: Nrf1, but not Nrf2, is targeted to the endoplasmic reticulum," *Biochemical Journal*, vol. 399, no. 3, pp. 373–385, 2006.
- [10] Y. Zhang, J. M. Lucocq, M. Yamamoto, and J. D. Hayes, "The NHB1 (N-terminal homology box 1) sequence in transcription factor Nrf1 is required to anchor it to the endoplasmic reticulum and also to enable its asparagine-glycosylation," *The Biochemical Journal*, vol. 408, no. 2, pp. 161–172, 2007.
- [11] Y. Zhang, Y. Ren, S. Li, and J. Hayes, "Transcription factor Nrf1 is topologically repartitioned across membranes to enable target gene transactivation through its acidic glucose-responsive domains," *PLoS One*, vol. 9, article e93456, 2014.
- [12] Y. Zhang and J. D. Hayes, "The membrane-topogenic vectorial behaviour of Nrf1 controls its post-translational modification and transactivation activity," *Scientific Reports*, vol. 3, article 2006, 2013.
- [13] Y. Zhang, S. Li, Y. Xiang, L. Qiu, H. Zhao, and J. D. Hayes, "The selective post-translational processing of transcription factor Nrf1 yields distinct isoforms that dictate its ability to differentially regulate gene expression," *Scientific Reports*, vol. 5, article 12983, 2015.
- [14] Y. Xiang, M. Wang, S. Hu et al., "Mechanisms controlling the multistage post-translational processing of endogenous Nrf1 $\alpha$ /TCF11 proteins to yield distinct isoforms within the coupled positive and negative feedback circuits," *Toxicology and Applied Pharmacology*, vol. 360, pp. 212–235, 2018.
- [15] Y. Xiang, J. Halin, Z. Fan et al., "Topovectorial mechanisms control the juxtamembrane proteolytic processing of Nrf1 to remove its N-terminal polypeptides during maturation of the CNC-bZIP factor," *Toxicology and Applied Pharmacology*, vol. 360, pp. 160–184, 2018.
- [16] A. Cuadrado, A. I. Rojo, G. Wells et al., "Therapeutic targeting of the NRF2 and KEAP1 partnership in chronic diseases," *Nature Reviews Drug Discovery*, vol. 18, no. 4, pp. 295–317, 2019.
- [17] K. Itoh, T. Chiba, S. Takahashi et al., "An Nrf2/Small Maf Heterodimer Mediates the Induction of Phase II Detoxifying Enzyme Genes through Antioxidant Response Elements," *Biochemical and Biophysical Research Communications*, vol. 236, no. 2, pp. 313–322, 1997.
- [18] K. Chan, R. Lu, J. C. Chang, and Y. W. Kan, "NRF2, a member of the NFE2 family of transcription factors, is not essential for murine erythropoiesis, growth, and development," *Proceedings of the National Academy of Sciences of the United States of America*, vol. 93, no. 24, pp. 13943–13948, 1996.
- [19] C. Xu, M. T. Huang, G. Shen et al., "Inhibition of 7,12-dimethylbenz(a)anthracene-induced skin tumorigenesis in C57BL/6 mice by sulforaphane is mediated by nuclear factor E2-related factor 2," *Cancer Research*, vol. 66, no. 16, pp. 8293–8296, 2006.
- [20] J. D. Hayes, M. McMahon, S. Chowdhry, and A. T. Dinkova-Kostova, "Cancer chemoprevention mechanisms mediated through the Keap1-Nrf2 pathway," *Antioxidants & Redox Signaling*, vol. 13, pp. 1713–1748, 2010.
- [21] H. Xiao, F. Lu, D. Stewart, and Y. Zhang, "Mechanisms underlying chemopreventive effects of flavonoids via multiple signaling nodes within Nrf2-ARE and AhR-XRE gene regulatory networks," *Current Chemical Biology*, vol. 7, no. 2, pp. 151–176, 2013.
- [22] M. Rojo de la Vega, E. Chapman, and D. D. Zhang, "NRF2 and the hallmarks of cancer," *Cancer Cell*, vol. 34, no. 1, pp. 21–43, 2018.
- [23] L. Qiu, M. Wang, S. Hu et al., "Oncogenic activation of Nrf2, though as a master antioxidant transcription factor, liberated by specific knockout of the full-length Nrf1 $\alpha$  that acts as a dominant tumor repressor," *Cancers*, vol. 10, p. 520, 2018.
- [24] J. Yuan, S. Zhang, and Y. Zhang, "Nrf1 is paved as a new strategic avenue to prevent and treat cancer, neurodegenerative and other diseases," *Toxicology and Applied Pharmacology*, vol. 360, pp. 273–283, 2018.
- [25] S. C. Farmer, C. W. Sun, G. E. Winnier, B. L. Hogan, and T. M. Townes, "The bZIP transcription factor LCR-F1 is essential for mesoderm formation in mouse development," *Genes & Development*, vol. 11, no. 6, pp. 786–798, 1997.
- [26] J. Y. Chan, M. Kwong, R. Lu et al., "Targeted disruption of the ubiquitous CNC-bZIP transcription factor, Nrf-1, results in anemia and embryonic lethality in mice," *The EMBO Journal*, vol. 17, no. 6, pp. 1779–1787, 1998.
- [27] M. Kwong, Y. W. Kan, and J. Y. Chan, "The CNC basic leucine zipper factor, Nrf1, is essential for cell survival in response to

- oxidative stress-inducing agents. Role for Nrf1 in gamma-gcs(l) and gss expression in mouse fibroblasts," *The Journal of Biological Chemistry*, vol. 274, no. 52, pp. 37491–37498, 1999.
- [28] Z. Xu, L. Chen, L. Leung, T. S. Yen, C. Lee, and J. Y. Chan, "Liver-specific inactivation of the Nrf1 gene in adult mouse leads to nonalcoholic steatohepatitis and hepatic neoplasia," *Proceedings of the National Academy of Sciences of the United States of America*, vol. 102, no. 11, pp. 4120–4125, 2005.
- [29] M. Ohtsuji, F. Katsuoka, A. Kobayashi, H. Aburatani, J. D. Hayes, and M. Yamamoto, "Nrf1 and Nrf2 play distinct roles in activation of antioxidant response element-dependent genes," *Journal of Biological Chemistry*, vol. 283, no. 48, pp. 33554–33562, 2008.
- [30] T. Tsujita, V. Peirce, L. Baird et al., "Transcription factor Nrf1 negatively regulates the cystine/glutamate transporter and lipid-metabolizing enzymes," *Molecular and Cellular Biology*, vol. 34, no. 20, pp. 3800–3816, 2014.
- [31] L. Leung, M. Kwong, S. Hou, C. Lee, and J. Y. Chan, "Deficiency of the Nrf1 and Nrf2 transcription factors results in early embryonic lethality and severe oxidative stress," *The Journal of Biological Chemistry*, vol. 278, no. 48, pp. 48021–48029, 2003.
- [32] H. Zheng, J. Fu, P. Xue et al., "CNC-bZIP protein Nrf1-dependent regulation of glucose-stimulated insulin secretion," *Antioxidants & Redox Signaling*, vol. 22, no. 10, pp. 819–831, 2015.
- [33] A. Kobayashi, T. Tsukide, T. Miyasaka et al., "Central nervous system-specific deletion of transcription factor Nrf1 causes progressive motor neuronal dysfunction," *Genes to Cells*, vol. 16, no. 6, pp. 692–703, 2011.
- [34] C. S. Lee, C. Lee, T. Hu et al., "Loss of nuclear factor E2-related factor 1 in the brain leads to dysregulation of proteasome gene expression and neurodegeneration," *Proceedings of the National Academy of Sciences of the United States of America*, vol. 108, no. 20, pp. 8408–8413, 2011.
- [35] Y.-P. Zhu, Z. Zheng, S. Hu et al., "Unification of opposites between two antioxidant transcription factors Nrf1 and Nrf2 in mediating distinct cellular responses to the endoplasmic reticulum stressor tunicamycin," *Antioxidants*, vol. 9, p. 4, 2019.
- [36] Y. Ren, L. Qiu, F. Lü et al., "TALENs-directed knockout of the full-length transcription factor Nrf1 $\alpha$  that represses malignant behaviour of human hepatocellular carcinoma (HepG2) cells," *Scientific Reports*, vol. 6, no. 1, article 23775, 2016.
- [37] P. D. McCrea and C. J. Gottardi, "Beyond  $\beta$ -catenin: prospects for a larger catenin network in the nucleus," *Nature Reviews Molecular Cell Biology*, vol. 17, no. 1, pp. 55–64, 2016.
- [38] M. J. Perugorria, P. Olaizola, I. Labiano et al., "Wnt- $\beta$ -catenin signalling in liver development, health and disease," *Nature Reviews Gastroenterology & Hepatology*, vol. 16, no. 2, article 75, pp. 121–136, 2019.
- [39] J. O. Russell and S. P. Monga, "Wnt/ $\beta$ -Catenin signaling in liver development, homeostasis, and pathobiology," *Annual Review of Pathology*, vol. 13, pp. 351–378, 2018.
- [40] J. C. Nault, S. Rebouissou, and J. Zucman Rossi, "NRF2/KEAP1 and Wnt/ $\beta$ -catenin in the multistep process of liver carcinogenesis in humans and rats," *Hepatology*, vol. 62, no. 3, pp. 677–679, 2015.
- [41] P. Zavattari, A. Perra, S. Menegon et al., "Nrf2, but not  $\beta$ -catenin, mutation represents an early event in rat hepatocarcinogenesis," *Hepatology*, vol. 62, no. 3, pp. 851–862, 2015.
- [42] S. Vilarinho, E. Z. Erson-Omay, A. S. Harmanci et al., "Paediatric hepatocellular carcinoma due to somatic CTNNB1 and NFE2L2 mutations in the setting of inherited bi-allelic ABCB11 mutations," *Journal of Hepatology*, vol. 61, no. 5, pp. 1178–1183, 2014.
- [43] S. A. Comerford, E. A. Hinnant, Y. Chen et al., "Hepatoblastoma modeling in mice places Nrf2 within a cancer field established by mutant  $\beta$ -catenin," *JCI Insight*, vol. 1, article e88549, 2016.
- [44] P. Rada, A. I. Rojo, A. Offergeld et al., "WNT-3A regulates an Axin1/NRF2 complex that regulates antioxidant metabolism in hepatocytes," *Antioxidants & Redox Signaling*, vol. 22, no. 7, pp. 555–571, 2015.
- [45] J. Yuan, H. Wang, Y. Xiang et al., "Nrf1D is the first candidate secretory transcription factor in the blood plasma, its precursor existing as a unique redox-sensitive transmembrane CNC-bZIP protein in hemopoietic and somatic tissues," *International Journal of Molecular Sciences*, vol. 19, no. 10, p. 2940, 2018.
- [46] M. Wang, L. Qiu, X. Ru, Y. Song, and Y. Zhang, "Distinct isoforms of Nrf1 diversely regulate different subsets of its cognate target genes," *Scientific Reports*, vol. 9, no. 1, article 2960, 2019.
- [47] G. M. Morriss and M. Solorsh, "Regional differences in mesenchymal cell morphology and glycosaminoglycans in early neural-fold stage rat embryos," *Development*, vol. 46, pp. 37–52, 1978.
- [48] P. Friedl and K. Wolf, "Tumour-cell invasion and migration: diversity and escape mechanisms," *Nature Reviews Cancer*, vol. 3, no. 5, pp. 362–374, 2003.
- [49] P. Sharma, Z. T. Bolten, D. R. Wagner, and A. H. Hsieh, "Deformability of human mesenchymal stem cells is dependent on vimentin intermediate filaments," *Annals of Biomedical Engineering*, vol. 45, no. 5, pp. 1365–1374, 2017.
- [50] R. Kalluri and R. A. Weinberg, "The basics of epithelial-mesenchymal transition," *The Journal of Clinical Investigation*, vol. 119, no. 6, pp. 1420–1428, 2009.
- [51] R. Nusse and H. Clevers, "Wnt/ $\beta$ -catenin signaling, disease, and emerging therapeutic modalities," *Cell*, vol. 169, pp. 985–999, 2017.
- [52] K. M. Loh, R. van Amerongen, and R. Nusse, "Generating cellular diversity and spatial form: Wnt signaling and the evolution of multicellular animals," *Developmental Cell*, vol. 38, no. 6, pp. 643–655, 2016.
- [53] V. Korinek, N. Barker, P. J. Morin et al., "Constitutive transcriptional activation by a beta-catenin-Tcf complex in APC-/- colon carcinoma," *Science*, vol. 275, no. 5307, pp. 1784–1787, 1997.
- [54] J. Steffen, M. Seeger, A. Koch, and E. Kruger, "Proteasomal degradation is transcriptionally controlled by TCF11 via an ERAD-dependent feedback loop," *Molecular Cell*, vol. 40, no. 1, pp. 147–158, 2010.
- [55] M. Shulewitz, I. Soloviev, T. Wu, H. Koeppen, P. Polakis, and C. Sakanaka, "Repressor roles for TCF-4 and Sfrp1 in Wnt signaling in breast cancer," *Oncogene*, vol. 25, no. 31, pp. 4361–4369, 2006.
- [56] L. Chen, M. Kwong, R. Lu et al., "Nrf1 is critical for redox balance and survival of liver cells during development," *Molecular and Cellular Biology*, vol. 23, no. 13, pp. 4673–4686, 2003.
- [57] S. K. Radhakrishnan, C. S. Lee, P. Young, A. Beskow, J. Y. Chan, and R. J. Deshaies, "Transcription factor Nrf1 mediates



- the proteasome recovery pathway after proteasome inhibition in mammalian cells," *Molecular Cell*, vol. 38, no. 1, pp. 17–28, 2010.
- [58] Z. Sha and A. L. Goldberg, "Proteasome-mediated processing of Nrf1 is essential for coordinate induction of all proteasome subunits and p97," *Current Biology*, vol. 24, no. 14, pp. 1573–1583, 2014.
- [59] C. S. Lee, D. V. Ho, and J. Y. Chan, "Nuclear factor-erythroid 2-related factor 1 regulates expression of proteasome genes in hepatocytes and protects against endoplasmic reticulum stress and steatosis in mice," *The FEBS Journal*, vol. 280, no. 15, pp. 3609–3620, 2013.
- [60] D. H. Oh, D. Rigas, A. Cho, and J. Y. Chan, "Deficiency in the nuclear-related factor erythroid 2 transcription factor (Nrf1) leads to genetic instability," *The FEBS Journal*, vol. 279, no. 22, pp. 4121–4130, 2012.
- [61] H. Haegel, L. Larue, M. Ohsugi, L. Fedorov, K. Herrenknecht, and R. Kemler, "Lack of beta-catenin affects mouse development at gastrulation," *Development*, vol. 121, no. 11, pp. 3529–3537, 1995.
- [62] P. Liu, M. Wakamiya, M. J. Shea, U. Albrecht, R. R. Behringer, and A. Bradley, "Requirement for Wnt3 in vertebrate axis formation," *Nature Genetics*, vol. 22, no. 4, pp. 361–365, 1999.
- [63] O. G. Kelly, K. I. Pinson, and W. C. Skarnes, "The Wnt coreceptors Lrp5 and Lrp6 are essential for gastrulation in mice," *Development*, vol. 131, no. 12, pp. 2803–2815, 2004.
- [64] J. Huelsken, R. Vogel, V. Brinkmann, B. Erdmann, C. Birchmeier, and W. Birchmeier, "Requirement for beta-catenin in anterior-posterior axis formation in mice," *The Journal of Cell Biology*, vol. 148, no. 3, pp. 567–578, 2000.
- [65] D. Hrckulak, L. Janeckova, L. Lanikova et al., "Wnt effector TCF4 is dispensable for Wnt signaling in human cancer cells," *Genes*, vol. 9, p. 439, 2018.
- [66] L. V. Nguyen, R. Vanner, P. Dirks, and C. J. Eaves, "Cancer stem cells: an evolving concept," *Nature Reviews Cancer*, vol. 12, no. 2, pp. 133–143, 2012.